An ancient RAB5 governs the formation of additional vacuoles and cell shape in petunia petals

Shuangjiang Li, Martina Cerri, Pamela Strazzer, Yanbang Li, Cornelis Spelt, Mattijs Bliek, Michiel Vandenbussche, Enric Martínez-Calvó, Biao Lai, Lara Reale, et al.

Cell Reports

Article

An ancient RAB5 governs the formation of additional vacuoles and cell shape in petunia petals

Graphical abstract

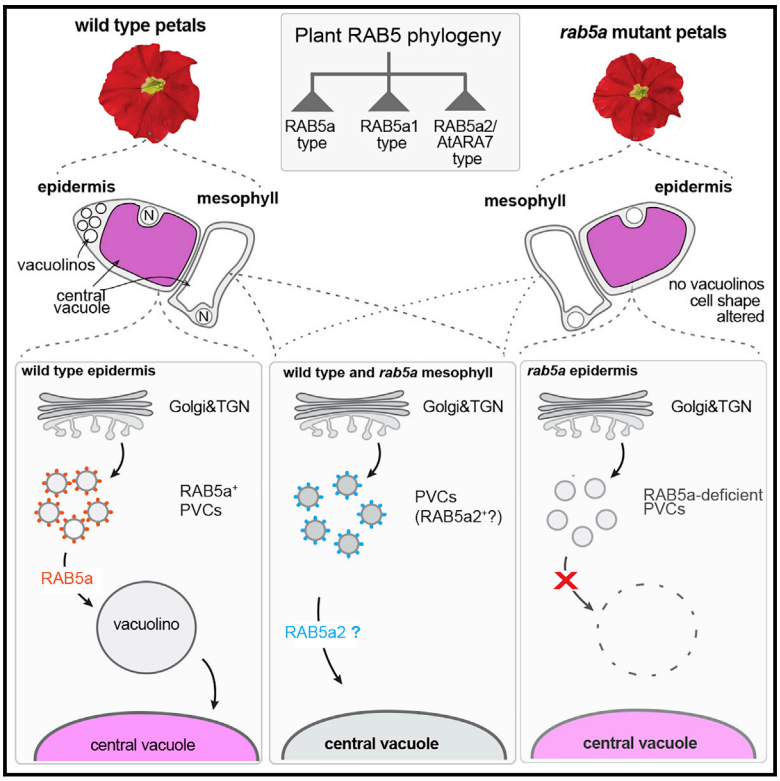

Highlights

- Flowering plants contain three ancient classes of canonical RAB5 proteins
- RAB5s display divergent transcription regulation and intracellular localization
- RAB5a is specifically required to form vacuolinos from small endosomal precursors
- The others, RAB5a1 and RAB5a2, cannot functionally replace RAB5a

Authors

Shuangjiang Li, Martina Cerri, Pamela Strazzer, ..., Lara Reale, Ronald Koes, Francesca M. Quattrocchio

Correspondence

ronald.koes@uva.nl

In brief

Flower petals contain small vacuolar compartments, named vacuolinos, that are intermediate stations for protein trafficking to the central vacuole. Li et al. report that petals express three distinct canonical RAB5 GTPases originating from ancient duplications and that one of these directs the formation of vacuolinos from small endosomal precursors.

Li et al., 2021, Cell Reports *36*, 109749
September 28, 2021
https://doi.org/10.1016/j.celrep.2021.109749

CellPress

Cell Reports

CellPress
OPEN ACCESS

Article

An ancient RAB5 governs the formation of additional vacuoles and cell shape in petunia petals

Shuangjiang Li,[1] Martina Cerri,[2] Pamela Strazzer,[1] Yanbang Li,[1] Cornelis Spelt,[1] Mattijs Bliek,[1] Michiel Vandenbussche,[3] Enric Martínez-Calvó,[1] Biao Lai,[1] Lara Reale,[2] Ronald Koes,[1,4,*] and Francesca M. Quattrocchio[1]

[1]Plant Development and (Epi)Genetics, Swammerdam Institute for Life Science, University of Amsterdam, Science Park 904, 1098 XH Amsterdam, the Netherlands

[2]Department of Agricultural, Food and Environmental Sciences, University of Perugia, Borgo XX Giugno 74, 06121 Perugia, Italy

[3]Laboratoire Reproduction et Développement des Plantes (RDP), ENS de Lyon/CNRS/INRA/UCBL, 46 Allée d'Italie, 69364 Lyon, France

[4]Lead contact

*Correspondence: ronald.koes@uva.nl

https://doi.org/10.1016/j.celrep.2021.109749

SUMMARY

Homologous ("canonical") RAB5 proteins regulate endosomal trafficking to lysosomes in animals and to the central vacuole in plants. Epidermal petal cells contain small vacuoles (vacuolinos) that serve as intermediate stations for proteins on their way to the central vacuole. Here, we show that transcription factors required for vacuolino formation in petunia induce expression of *RAB5a*. RAB5a defines a previously unrecognized clade of canonical RAB5s that is evolutionarily and functionally distinct from ARA7-type RAB5s, which act in trafficking to the vacuole. Loss of RAB5a reduces cell height and abolishes vacuolino formation, which cannot be rescued by the ARA7 homologs, whereas constitutive RAB5a (over)expression alters the conical cell shape and promotes homotypic vacuolino fusion, resulting in oversized vacuolinos. These findings provide a rare example of how gene duplication and neofunctionalization increased the complexity of membrane trafficking during evolution and suggest a mechanism by which cells may form multiple vacuoles with distinct content and function.

INTRODUCTION

In all eukaryotes, membrane traffic is an essential process that delivers proteins and other compounds to distinct cellular compartments by membrane vesicles that bud off from donor membranes to fuse with specific target compartments. SNARE proteins and RAB GTPases are major factors in determining the identity of vesicles/endosomes and their fusion with membranes from specific target compartments. SNAREs, RABs, and other trafficking regulators are encoded by gene families that existed in early eukaryotes. Since the separation of animals and plants, these families have expanded by independent gene duplications in both lineages, which is thought to have been important for the increased tissue specificity and complexity of trafficking systems during evolution. However, specific examples supporting this idea remain scarce.

Secretion is a major trafficking pathway that delivers proteins to the plasma membrane or, when the protein has a specific vacuolar sorting domain, to the vacuole or lysosome. Although many plant cells contain a single vacuole, several cell types possess multiple vacuoles with different content and, apparently, different functions (Epimashko et al., 2004; Fleurat-Lessard et al., 1997; Frigerio et al., 2008; Otegui et al., 2005; Paris et al., 1996). Cells in the epidermis of flower petals are dedicated to attracting animal pollinators by visual (color) and/or chemical (scent) cues and by providing a landing site. In petunia and roses, these cells contain a large central vacuole (CV) filled with anthocyanin pigments, as well as numerous small vacuolar compartments, called vacuolinos (Figure 1A), that lack anthocyanins (Faraco et al., 2017).

In petunia flowers, a complex of transcription factors (MYB-bHLH-WD40, MBW), which consists of the MYB protein ANTHOCYANIN2, the bHLH protein AN1, and the WD40 protein AN11, drives the expression of genes involved in anthocyanin synthesis in late stages of bud development, prior to opening of the flower (de Vetten et al., 1997; Quattrocchio et al., 1999, 2006; Spelt et al., 2000). Slightly later, when the bud has reached its maximum size and the flower opens, a related MYB-bHLH-WD40-WRKY (MBWW) complex, consisting of the MYB protein PH4, AN1, AN11, and the WRKY factor PH3, activates a (partially) distinct set of target genes, which drive the hyper-acidification of the CVs in colored cells of the petal epidermis to confer a red-violet flower color (Quattrocchio et al., 2006; Spelt et al., 2000; Verweij et al., 2016) and the formation of vacuolinos (Faraco et al., 2017). The major target genes involved in vacuolar acidification, namely, *PH1* and *PH5*, encode two interacting P-ATPases that reside in the CV membrane (tonoplast) and act as a proton pump (Faraco et al., 2014; Verweij et al., 2008).

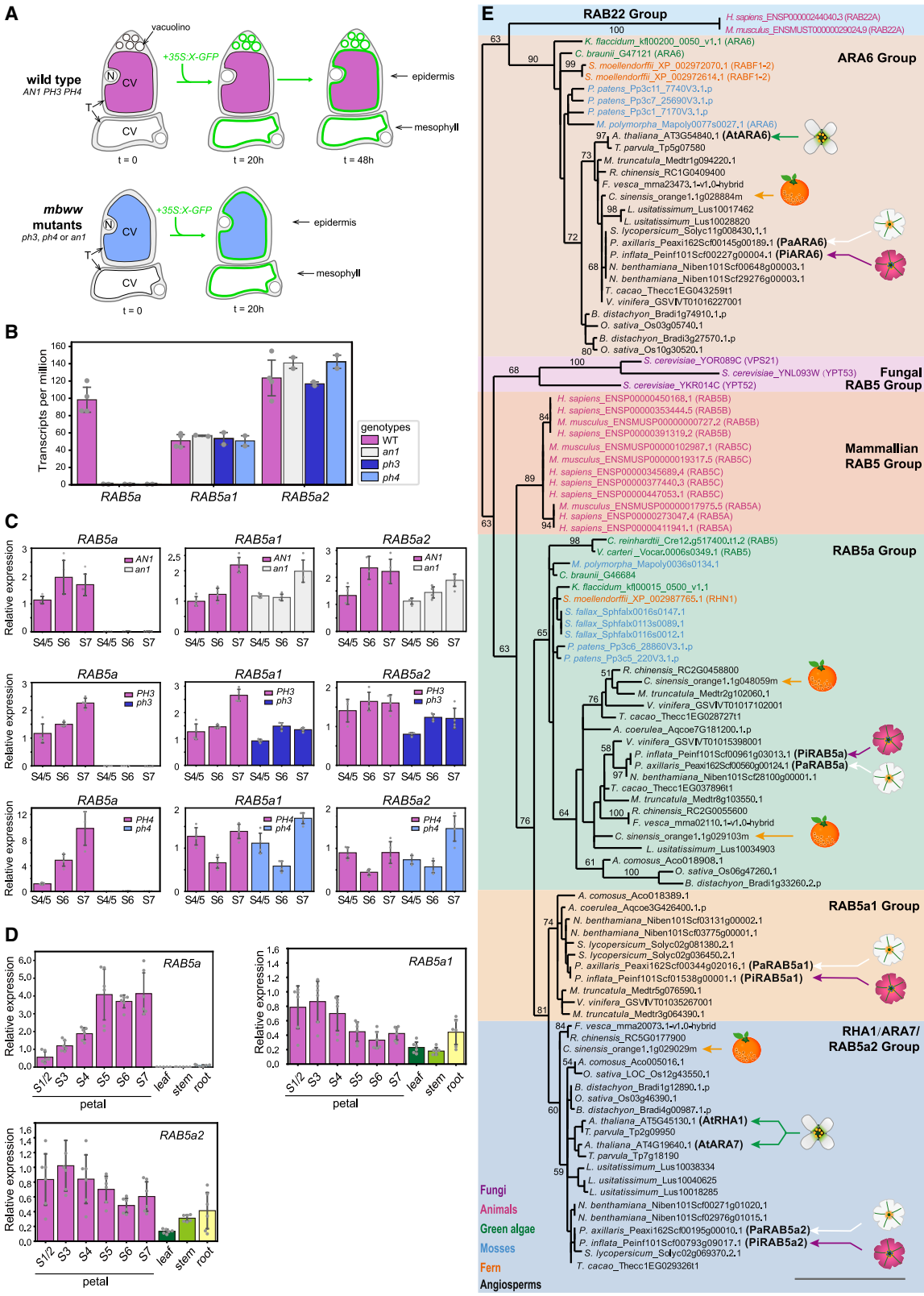

(legend on next page)

However, no MBWW-regulated genes involved the in formation of vacuolinos have been identified thus far.

Vacuolinos represent an intermediate station for membrane proteins, like PH1, PH5, KCO1, vacuolar SNAREs, and soluble proteins, such as Aleu green fluorescent protein (Aleu-GFP), on their way to the CV (Figure 1A). In transient expression assays, these proteins accumulate first in vacuolinos, after about 24 h, before they arrive at the CV, after approximately 48 h (Faraco et al., 2017). In epidermal petal cells of *an1*, *ph3*, and *ph4* mutants, which lack vacuolinos, proteins move "directly" (within 24 h) to the CV, as they do in wild-type petal mesophyll and leaf cells (Faraco et al., 2017; Figure 1A). The MBWW target gene *PH1* is essential for the trafficking from vacuolinos to the CV, as in *ph1* mutant petals vacuolar proteins accumulate in (enlarged) vacuolinos but do not move on to the CV (Faraco et al., 2017). This suggests that both the formation of vacuolinos and the transport from vacuolinos to the CV require a largely unknown set of factors that are encoded by MBWW-regulated genes.

GTPases of the RAB family are regulators of endomembrane trafficking in all eukaryotes (Uemura and Ueda, 2014; Wandinger-Ness and Zerial, 2014). They cycle between an inactive guanosine diphosphate (GDP)-bound and an active guanosine triphosphate (GTP)-bound form that is attached to the membrane where they recruit specific effectors (Barr and Lambright, 2010; Langemeyer et al., 2018; Müller and Goody, 2018). *Arabidopsis* possesses two "canonical" RAB5s, namely, RHA1 and ARA7 (also called RABF2a and RABF2b), that are orthologous to metazoan RAB5s and a more distant relative, ARA6 (also called RABF1), belonging to a plant-specific clade of RAB5s (Rutherford and Moore, 2002; Vernoud et al., 2003). ARA7, RHA1, and ARA6 are converted from the GDP-bound to the GTP-bound form by the same activator, the Guanine nucleotide Exchange Factor (GEF) VPS9a (Fukuda et al., 2013; Goh et al., 2007; Sunada et al., 2016) and, to a lesser extent, the redundant paralog VPS9b (Nielsen and Thordal-Christensen, 2018). Yet, they have different functions. ARA7 and RHA1 localize to nearly identical populations of prevacuolar compartments (PVCs)/multivesicular bodies (MVBs) and are involved in vacuolar trafficking in leaf and root cells (Bottanelli et al., 2012; Kotzer et al., 2004; Lee et al., 2004; Sohn et al., 2003) and to specific defense structures (encasements) in pathogen-infected cells (Nielsen et al., 2017), whereas ARA6 resides on a subpopulation of endosomes partially overlapping with ARA7/RHA1 positive ones and functions mainly in the traffic between PVCs/MVBs and the plasma membrane (Ebine et al., 2011; Ueda et al., 2004).

In this study, we found that petals from an opening petunia flower express three canonical *RAB5* genes, namely, *RAB5a*, *RAB5a1*, and *RAB5a2*. RAB5a2 is orthologous to the well-studied RHA1 and ARA7 from *Arabidopsis*, whereas RAB5a and RAB5a1 represent evolutionary distinct clades that are missing in *Arabidopsis* and thus were not previously recognized. Evolutionary divergence is mirrored by profound differences in their transcriptional regulation, intracellular localization, and biological function. We show that *RAB5a* expression is activated by AN1, PH3, and PH4 and is required for the formation of vacuolinos.

RESULTS

Identification of three canonical RAB5 homologs in petunia

Examination of RNA sequencing (RNA-seq) data indicated that petunia petals express three canonical *RAB5* genes, namely, *RAB5a*, *RAB5a1*, and *RAB5a2* (Figure 1B; Figure S1A). *RAB5a* is expressed primarily in petals and in the vasculature of leaves and stems and is strongly reduced in *an1*, *ph3*, and *ph4* mutant petals (Figures 1B–1D; Figure S1B), suggesting a role in the vacuolino pathway. *RAB5a1* and *RAB5a2*, by contrast, are not controlled by *AN1*, *PH3*, or *PH4* (Figures 1B and 1C) and are expressed in a broad range of tissues (Figure 1D).

To examine the relationship of these petunia proteins with the canonical *Arabidopsis* RAB5s (ARA7 and RHA1) and AtARA6, which belongs to a distinct plant-specific clade of RAB5-like proteins, we retrieved highly similar proteins from genome databases and performed phylogenetic analyses (Figure 1E). These analyses revealed that the petunia protein PhARA6 is the apparent ortholog of ARA6, which in this and other analyses is more related to RAB22 than to RAB5s, whereas RAB5a, RAB5a1, and RAB5a2 are canonical RAB5s that are co-orthologs of animal RAB5s (Figure 1E). The canonical plant RAB5s proved more diverse than previously thought. RAB5a2 is apparently orthologous to ARA7 and RHA1 from *Arabidopsis*, whereas RAB5a1 and RAB5a represent two distinct clades. These three clades existed already in early angiosperms because distantly related Eudicot species belonging to Asterids

Figure 1. Identification and characterization of three *RAB5* genes in petunia

(A) Diagrams showing vacuolar compartments (vacuolinos and central vacuole) and localization of anthocyanins (purple) and transiently expressed vacuolar proteins tagged with green fluorescent protein (X-GFP, green) in epidermal and mesophyll cells of wild-type (WT) and of mutant petals lacking one of the components of the MBWW transcription factor complex. N, nucleus; CV, central vacuole; T, tonoplast; X, vacuolar protein; t, time after transient transfection.

(B) Transcript reads for *RAB5a*, *RAB5a1*, and *RAB5a2* per million transcripts from RNA-seq analysis of petals from *an1*, *ph3*, *ph4*, and WT plants. Values are presented as mean ± SD; n = 2 biological replicates for each of the mutants (*an1*, *ph3*, and *ph4*); and 4 biological replicates for WT.

(C) Quantitative real-time PCR analysis of *RAB5a*, *RAB5a1*, and *RAB5a2* expression in petals of *an1*, *ph4*, *ph3*, and WT flowers in (pooled) developmental stages 1–4 (10-mm to 35-mm flower buds), 5 (maximum-length flower buds), 6 (opened flower, prior to anthesis), and 7 (2 days after flower opening). Values (mean ± SD) are based on 2 biological replicates (each with 2 technical replicates) and are standardized based on *PhRAN*.

(D) Quantitative real-time PCR analysis of the expression of *RAB5a*, *RAB5a1*, and *RAB5a2* in petals (stages defined as in C), leaves, stems, and roots of the WT petunia line M1xV30. Values are presented as mean ± SD; n = 3 biological replicates × 2 technical replicates in all cases.

(E) Phylogenetic analysis of RAB5 proteins from different organisms. The tree is built by maximum likelihood, and branch support is indicated as percentage of 300 bootstraps if ≥50%. The positions of RAB5 homologs from *Arabidopsis* and *Petunia axillaris* and *Petunia inflata,* the wild species from which *P. hybrida* originates; and *Citrus* are indicated by the cartoons of flowers and fruit, respectively. Distinct RAB clades are given different colors as indicated on the right. See also Figure S1.

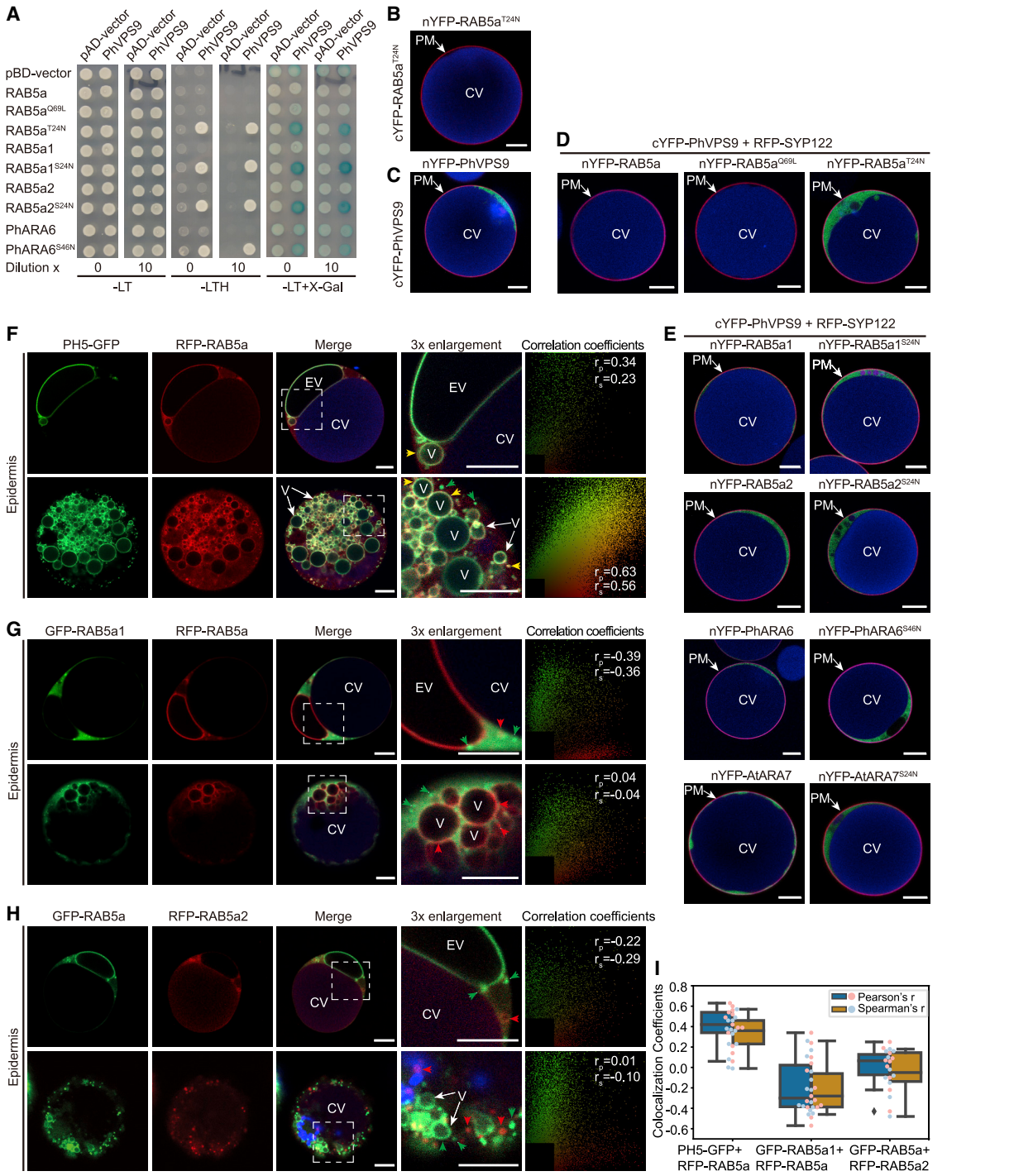

Figure 2. RAB5 proteins bind the same GEF but localize in different cell compartments

(A) Yeast two-hybrid assays indicate the interaction between GAL4^{BD} fusions of WT and mutant versions of RAB5s and a GAL4^{AD} fusion of PhVPS9a.

(B–E) Split YFP assays confirming the interaction of RAB5 proteins with PhVPS9a in cells from petunia petal epidermis. Transformed cells are marked by (co-) expression of the plasma membrane protein RFP-SYP122. (B) Negative control showing that reassociation of nYFP and cYFP moieties fused to non-interacting proteins (RAB5a^{T24N}) is negligible (n = 29 cells). (C) Positive control showing that PhVPS9a oligomerizes, like AtVPS9a (n = 21 cells). (D) PhVPS9a interacts with RAB5a^{T24N} (n = 61 cells) but not, or much less, with RAB5a (n = 23 cells) or RAB5a^{Q69L} (n = 19 cells). (E) Interaction of *Petunia* RAB5 homologs and *Arabidopsis* RAB5 (AtARA7) with PhVPS9a (n = 13 to 33 cells).

(F) Confocal micrographs of WT petal protoplasts co-expressing RFP-RAB5a and PH5-GFP representing two types of cells with enlarged vacuolino (top) or normal-sized vacuolinos (bottom). Yellow arrowheads indicate co-localization; green arrowheads indicate the absence of co-localization. Co-localization, or lack thereof, in the micrographs is quantified in the scatterplots on the right (r_p, Pearson's r; r_s, Spearman's r).

(legend continued on next page)

(e.g., petunia and *Solanum lycopersicum*), Rosids (e.g., *Vitis vinifera* and *Medicago truncatula*), and Ranunculales (*Aquilegia caerulea*), as well as monocot species (e.g., *Oryza sativa* and *Ananas comosus*), all possess homologs of RAB5a, RAB5a1, and RHA1/ARA7/RAB5a2 (Figure 1E). Thus, the absence of RAB5a and RAB5a1 homologs in *Arabidopsis* and related Brassicaceae is most likely due to gene loss in the lineage that gave rise to these species.

In early diverging plant lineages, such as the bryophytes *Physcomitrella patens* and *Sphagnum fallax*; the liverwort *Marchantia polymorpha*; the algae *Klebsormidium flaccidum*, a Charophyte; and *Chlamydomonas reinhardtii* and *Volvox carteri*, two Chlorophytes, no such diversification of RAB5s is found, as these proteins cluster in a single clade. Surprisingly, this clade is more similar to the angiosperm RAB5a homologs than to RAB5a1 or RHA1/ARA7/RAB5a2 homologs. The process by which daughters of a gene duplication accumulate sequence changes at uneven rates is known as ''asymmetric evolution'' and is at least in some cases associated with the acquisition of new molecular functions by the faster diverging daughters (Holland et al., 2017). This suggests that the molecular function of the angiosperm RAB5a homologs (e.g., in terms of the effectors on which they act) may be more similar to that of their progenitors in basal plants, whereas the more diverged homologs from the RHA1/ARA7/RAB5a2 and RAB5a1 clades acquired distinct (molecular) functions that may involve distinct effectors.

All three petunia RAB5 homologs interact with the GEF PhVPS9

To assess the functional differences and similarities between the petunia RAB5s, we analyzed their interaction with a candidate GEF activator(s) (Herman et al., 2018). All known GEFs that activate RAB5s share a conserved domain (VPS9) (Carney et al., 2006). Although animals, fungi, and non-flowering plants can have up to five types of VPS9-domain-containing proteins, flowering plants have only one type (Herman et al., 2018; Letunic et al., 2021) that is encoded by two closely related and functionally redundant paralogs in *Arabidopsis* (*AtVPS9a* and *AtVPS9b*) (Goh et al., 2007; Nielsen et al., 2017; Nielsen and Thordal-Christensen, 2018) or a single gene in petunia (*PhVPS9*) and many other species (Figure S1C). In GAL4-based yeast two-hybrid assays, we observed little or no interaction between PhVPS9-GAL4^{AD} and GAL4^{BD} fusions of various RAB5s (Figure 2A), which was expected because in yeast RABs are thought to be mostly in their active GTP-bound form (Goh et al., 2007). Therefore, we examined interactions of PhVPS9 with the GDP-fixed mutants RAB5a^{T24N}, RAB5a1^{S24N}, RAB5a2 ^{S24N}, and PhARA6^{S46N}, which cannot be converted into the active GTP-bound form (Carney et al., 2006), and we found positive interactions in all cases (Figure 2A). The GTP-fixed mutant RAB5a^{Q69L}, by contrast, could not bind PhVPS9 (Figure 2A).

To examine these interactions in petunia petal cells, we performed bimolecular fluorescence complementation (BiFC), using split-yelllow fluoescent protein (YFP) assays. In protoplasts originating from the petal epidermis or petal mesophyll, which can be distinguished by the presence or absence of anthocyanin pigments in their CVs, respectively (Faraco et al., 2011), co-expression of nYFP-RAB5a^{T24N} and cYFP-RAB5a^{T24N} fusions did not result in noticeable YFP fluorescence (Figure 2B; Figure S1D), indicating that spontaneous reconstitution of YFP is negligible in these cells. Oligomerization of nYFP-PhVPS9 and cYFP-PhVPS9 was readily detectable (Figure 2C; Figure S1E), consistent with previous findings on AtVSP9a (Sunada et al., 2016). In line with the yeast two-hybrid results, we observed that cYFP-PhVPS9 interacted with GDP-fixed nYFP-RAB5a^{T24N} in cells from the petal epidermis and the mesophyll, but not, or much less, with GTP-fixed nYFP-RAB5a^{Q69L} or wild-type nYFP-RAB5a (Figure 2D; Figure S1F). We obtained essentially similar results with native and GDP-fixed forms of RAB5a1 (Figure 2E; Figure S1G), whereas RAB5a2, its paralog AtARA7, and PhARA6 interacted with PhVSP9 in both their GDP-fixed and the wild-type form (Figure 2E; Figure S1G).

These results indicate that the three distinct canonical RAB5s, as well as PhARA6, can bind to and may potentially compete for the same GEF activator PhVPS9.

Intracellular localization of RAB5s

We compared the intracellular localization of the three petunia RAB5s by using fusions to fluorescent proteins (FPs). A considerable number of FP fusion proteins undergo cleavage in plant cells because of which the separated moieties containing the FP and the tagged protein may localize to different compartments or undergo differential turnover (Quattrocchio et al., 2013). In such cases, the FP fluorescence does not reliably report the whereabouts of the tagged protein, even when expression of the FP fusion protein efficiently complements a mutant phenotype (Quattrocchio et al., 2013). Therefore, we analyzed GFP-RAB5a, GFP-RAB5a1, and GFP-RAB5a2 by immuno-blot analysis and found that these fusion proteins remain intact in petal cells (Figure S2A). Together with the finding that GFP-RAB5a can functionally substitute for native RAB5a in the rescue of vacuolino formation in a *rab5a* mutant and the enlargement of vacuolinos in protoplasts and transgenic plants (see below), this indicates that GFP-RAB5a fluorescence reliably reports RAB5a trafficking and localization.

To assess the localization of RAB5a in wild-type (M1xV30) petal cells, we transiently co-expressed RFP-RAB5a (red fluorescent protein-RAB5a) with PH5-GFP (Figure 2F; Figure S2B),

(G and H) Confocal micrographs of WT petal protoplasts co-expressing GFP-RAB5a1 and RFP-RAB5a (G) and GFP-RAB5a and mRFP-RAB5a2 (H). Two epidermal cells are shown representing cells with an enlarged vacuolino (top) or normal-sized vacuolinos (bottom).

(I) r_p and r_s correlation coefficients for co-localization of RFP-RAB5a and PH5-GFP (n = 13 cells), GFP-RAB5a1 and RFP-RAB5a (n = 14 cells), and GFP-RAB5a and RFP-RAB5a2 (n = 10 cells). Boxplot elements: center line, median; box limits, upper and lower quartiles; whiskers, 1.5× interquartile range; diamonds, outliers.

In (B) to (H), the autofluorescence of anthocyanins is shown in blue, fluorescence of RFP in red, and fluorescence of GFP in green. Bars represent 10 μm in all panels; 3× enlargement shows the region marked by the white dashed square at a 3-fold larger magnification. Abbreviations: PM, plasma membrane; V, vacuolino; EV, enlarged vacuolino. See also Figures S2–S5.

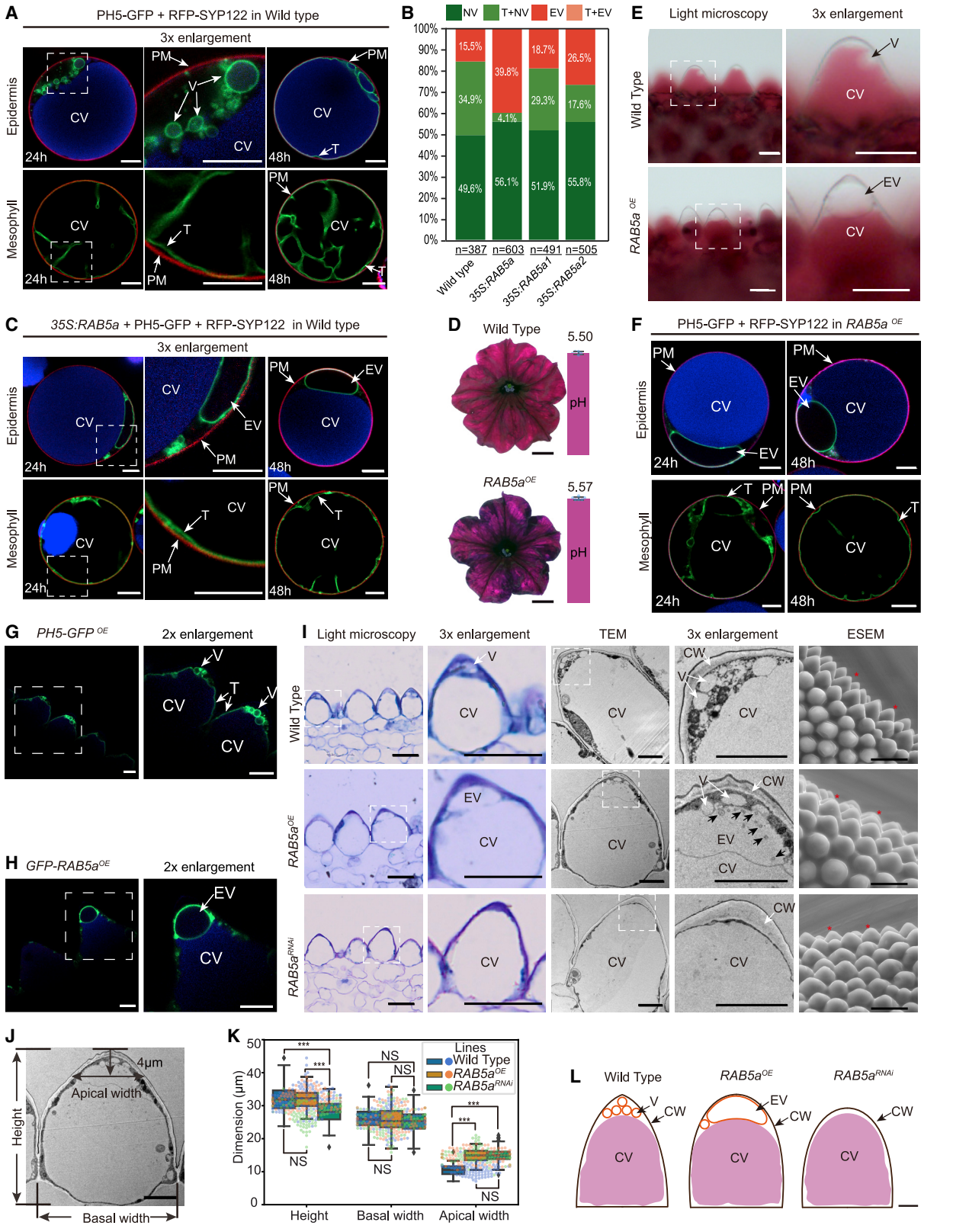

(legend on next page)

which marks the tonoplast and vacuolino membrane, or Aleu-GFP (Figure S2C), which marks the lumen of the CV and vacuolinos (Faraco et al., 2017). In protoplasts from the petal epidermis, RFP-RAB5a accumulated in the cytoplasm, the membrane of vacuolinos, and smaller compartments (puncta) that also contain PH5-GFP and Aleu-GFP and might represent PVCs (Figure 2F; Figure S2C). However, RFP-RAB5a was not seen in all PH5-GFP-positive puncta (see green arrowhead in the lower cell in Figure 2F), suggesting that these represent a partially distinct population (or maturation stages) of compartments. Cytoplasmic RFP-RAB5a is likely to be in the (inactive) GDP-bound state, whereas membrane-bound RFP-RAB5a is in the (active) GTP-bound state (Barr and Lambright, 2010; Müller and Goody, 2018). Also in petal mesophyll protoplasts, which lack anthocyanins and vacuolinos, RFP-RAB5a localized in puncta, partially overlapping with the puncta marked by PH5-GFP (Figure S2B).

To compare the subcellular localization of RAB5a, RAB5a1, and RAB5a2 proteins, we transiently co-expressed fusion proteins tagged with RFP or GFP in wild-type (M1xV30) petal protoplasts and assessed colocalization by Pearson's r and Spearman's correlation analysis (Figures 2G and 2H; Figures S2D and S2E). GFP-RAB5a and RFP-RAB5a accumulated in similar patterns in epidermal cells and in mesophyll cells too, but the fluorescence of RFP-RAB5a was considerably weaker than that of GFP-RAB5a (Figure S2D). GFP-RAB5a1 localized in epidermal cells in the cytoplasm and small punctate compartments that do not overlap with RFP-RAB5a-positive puncta or vacuolinos (Figure 2G). RFP-RAB5a2 localized to the cytoplasm and to punctate compartments that are distinct from puncta containing GFP-RAB5a (Figure 2H). Interestingly, also, GFP-RAB5a1 and RFP-RAB5a2 labeled in epidermal petal cells distinct populations of puncta, with little or no overlap (Figure S2G). In petal mesophyll cells, which lack vacuolinos, the same RAB5a, RAB5a1, and RAB5a2 fusions also accumulated in the cytoplasm and distinct populations of puncta (Figures S2E and S2F). Taken together, our results show that the localization of RAB5a partially overlaps with that of PH5 and hardly, if at all, with RAB5a1 and RAB5a2 (Figure 2I).

Next, we examined the identity of the GFP-RAB5a-positive puncta by using markers for the endoplasmic reticulum (ER) (RFP-KDEL; Fluckiger et al., 2003), *cis*-Golgi (ERD2-RFP; Silva-Alvim et al., 2018), *trans*-Golgi network/early endosomes (TGN/EE) (RFP-LeRAB11; Rehman et al., 2008), and PVCs/MVBs (CHERRY-BP80; De Benedictis et al., 2013). In epidermal petal cells, we observed no co-localization of GFP-RAB5a with ERD2-RFP, RFP-LeRAB11, or RFP-KDEL (Figures S3A, S3B, and S4A). GFP-RAB5a-positive puncta partially overlapped with CHERRY-BP80-positive compartments (Figure S3C), suggesting that they are a subpopulation of PVC-like compartments. Furthermore, GFP-RAB5a localized with CHERRY-BP80 in vacuolinos (Figure S3C). Interestingly, CHERRY-BP80, or at least its FP-tag, seems to become soluble in vacuolinos and to accumulate in the vacuolino lumen rather than the membrane (Figure S3C). In petal mesophyll cells, where RAB5a is normally not expressed, we observed partial co-localization of GFP-RAB5a with CHERRY-BP80 (Figure S3C) and with RFP-KDEL (Figure S4A), indicating that in mesophyll cells, part of GFP-RAB5a is localized in or close to the ER and to PVCs. It is unlikely that the association of RAB5a with the ER is caused by the absence of vacuolinos, as we found no co-localization of GFP-RAB5a and RFP-KDEL in epidermal cells from *ph3* and *ph4* mutant petals, which lack vacuolinos (Figures S4B and SC). As RAB5a is normally not expressed in the petal mesophyll, the association of GFP-RAB5a with the ER in these cells has no apparent biological relevance and was not investigated further.

In *Arabidopsis* cells, AtARA6 and AtARA7-positive PVCs/MVBs become labeled within 30 min after addition of the

Figure 3. Constitutive RAB5a expression blocks vacuolino-to-CV transport and alters cell shape

(A) Transient expression of PH5-GFP labels vacuolinos with normal size (24 h) and reaches tonoplast (48 h) in WT (M1xV30) petal protoplasts. The number of epidermal cells imaged at 24 h ($n_{epi\text{-}24h}$) and 48 h ($n_{epi\text{-}48h}$) is 97 and 33, respectively; mesophyll cells imaged at 24 h ($n_{mes\text{-}24h}$) and 48 h ($n_{mes\text{-}48h}$) is 26 and 15, respectively.Scale bars, 10 μm.

(B) Percentage of cells with enlarged vacuolinos and/or tonoplast localization of PH5-GFP after transient expression of *RAB5a*, *RAB5a1*, and *RAB5a2* for 48 h. NV, normal-sized vacuolino (1–10 μm); T+ NV, cells with PH5-GFP on both tonoplast and normal-sized vacuolinos; T+ EV, cells with PH5-GFP on both tonoplast and enlarged vacuolino (such cells were not observed).

(C) Transient expression of *RAB5a* in WT (M1xV30) petal protoplasts induces the formation of enlarged vacuolinos ($n_{epi\text{-}24h}$ = 19, $n_{mes\text{-}24h}$ = 3, $n_{epi\text{-}48h}$ = 32, and $n_{mes\text{-}48h}$ = 10 cells). Scale bars, 10 μm.

(D) Flower phenotype and pH value of the petal extracts (n = 6 flowers) of WT and transgenic *RAB5a*^{OE} plants (bars, 1 cm).

(E) Light micrographs of epidermal cells from WT and *RAB5a*^{OE} petals. Red, anthocyanins; scale bars, 20 μm.

(F) Confocal micrograph of protoplasts from *RAB5a*^{OE} petals, transiently expressing PH5-GFP and RFP-SYP122 ($n_{epi\text{-}24h}$ = 50, $n_{mes\text{-}24h}$ = 11, $n_{epi\text{-}24h}$ = 15, and $n_{mes\text{-}24h}$ = 3 cells). Scale bars, 10 μm.

(G and H) Confocal images of petals from transgenic WT (M1xV30) plants expressing *35S:PH5-GFP* (*PH5-GFP*^{OE}) (G) or *35S:GFP-RAB5a* (*GFP-RAB5a*^{OE}) (H). 2× Enlargement refers to the portion of the image contained in the white dashed square. Bars, 10 μm.

(I) Light micrographs and transmission electron micrographs (TEMs) of petals sections and environmental scanning electron micrographs (ESEMs) of the surface of WT, *RAB5a*^{OE}, and *RAB5a*^{RNAi} petals. Scale bars for light microscopy are 20 μm, for TEM are 5 μm, and for ESEM are 50 μm. Red asterisks mark the tip of the cells, and black arrows mark ILVs.

(J) EM micrograph depicting how height, basal width, and apical width (width at 4 μm below the cell tip) of epidermal cells were measured.

(K) Dimensions of epidermal cells from different lines (height and basal width, n > 100 cells; apical width, n > 80 cells). Boxplot elements: center line, median; box limits, upper and lower quartiles; whiskers, 1.5× interquartile range; diamonds, outliers. Statistical significance was assessed by Student's t test/Mann-Whitney rank sum test; ***p < 0.001; NS, not significant.

(L) Simplified model of the effect of altered RAB5a expression on dimensions and shape of petal epidermal cells of the same genotypes as above.

Autofluorescence of anthocyanins in the CV of epidermal cells and chloroplasts in mesophyll cells is shown in blue, fluorescence of RFP-SYP122 in red, and fluorescence of PH5-GFP and GFP-RAB5a in green. 3× Enlargement shows the region marked by the white dashed square at 3-fold higher magnification. Abbreviation: CW, cell wall. See also Figure S6.

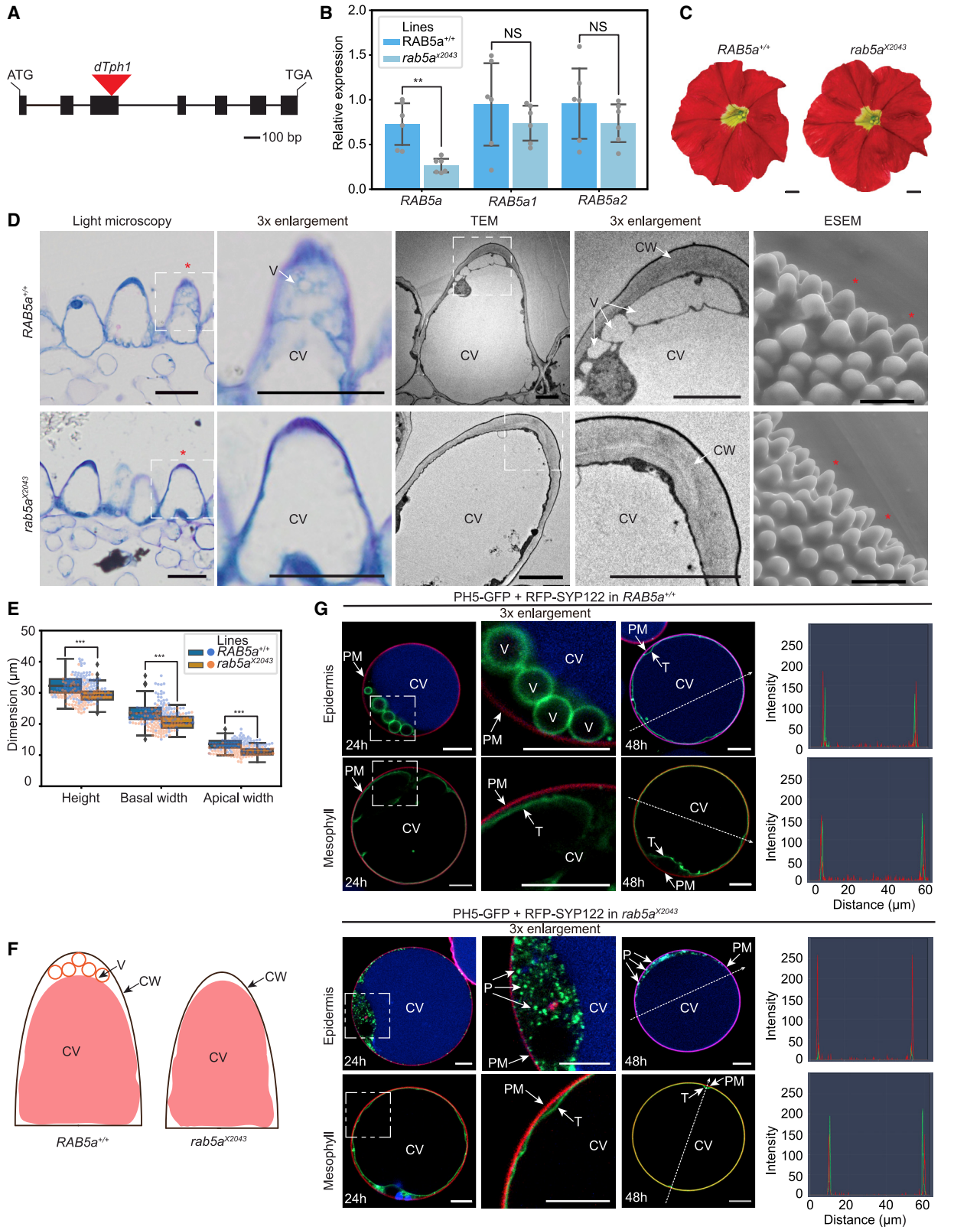

(legend on next page)

endocytic tracker FM4-64, indicating that they are intermediates in an endocytic pathway (Ueda et al., 2001, 2004). In petunia protoplasts from the petal mesophyll and the epidermis, FM4-64 is also rapidly endocytosed and after 10 min labels numerous endosomes that are distinct from the GFP-RAB5a-positive punctate compartments and vacuolinos (Figure S5). After 1 h, the punctate FM4-64-positive and GFP-RAB5a-positive compartments remained separate populations, whereas co-localization of FM4-64 and GFP-RAB5a became evident on vacuolinos, which increased further in time (Figure S5).

These findings suggest that (1) the RAB5a-positive puncta in epidermal petals cells are PVC-like compartments, which are distinct from the PVC/MVBs involved in endocytic pathway or the "direct" AtARA7 (RAB5a2)-dependent pathway to the CV and (2) that vacuolinos may be the station in epidermal petal cells where the endocytic pathway and vacuolino pathway merge.

Effects of constitutive RAB5a expression

We noticed that vacuolinos labeled by transiently expressed GFP-RAB5a were often much larger than those in cells expressing other GFP-tagged proteins. To further investigate this finding, we transiently co-expressed native RAB5a with PH5-GFP from the *35S* promoter in wild-type (M1xV30) petal protoplasts. When expressed alone in epidermal petal cells, PH5-GFP localized 24 h after transformation on vacuolinos with a normal size (1–10 μm in diameter) and reached the CV after 48 h in ~35% of the cells (Figures 3A and 3B), as described previously (Faraco et al., 2017). However, when co-expressed in epidermal petal cells with *35S:RAB5a*, PH5-GFP localized after 24 h in vacuolinos, which were in many cells much larger than those in cells expressing PH5-GFP alone (Figure 3C). After 48 h, PH5-GFP reached the CV in only 4% of the epidermal cells, which all had vacuolinos of a normal size (1–10 μm), whereas PH5-GFP did not reach the CV in in any of the cells with enlarged vacuolinos (>10 μm) (Figures 3B and 3C). In the same cells, the sorting of the plasma membrane marker RFP-SYP122 was not affected by *35S:RAB5a* (Figure 3C). In addition, *35S:RAB5a* had no noticeable effect on the trafficking of PH5-GFP to the CV in petal mesophyll cells either (Figure 3C). This result indicates that constitutive *RAB5a* (over)expression from the *35S* promoter affects only the pathway from vacuolinos to the CV. Interestingly, *35S:RAB5a2* also resulted in cells with enlarged vacuolino(s) and blocked transport to the CV, although with lower frequency (26.5%) than *35S:RAB5a* (40%), whereas *35S:RAB5a1* had little or no effect (Figure 3B).

Next, we generated 40 transgenic wild-type (M1xV30) plants containing *35S:RAB5a* and analyzed the phenotype of the six plants (*RAB5a*^{OE}) that (over)expressed *RAB5a* mRNA (Figure S6A). When *RAB5a*^{OE} flowers opened, most of the petal tissue had a blue-violet color and acquired its normal red-violet color only at later stages (Figure 3D; Figure S6B). The blue-violet flower color is typical of *ph* mutants and is caused by the reduced acidity of the CV, where anthocyanin pigments reside, due to impaired expression of the proton pumping PH1-PH5 complex in the tonoplast (Faraco et al., 2014; Verweij et al., 2008). Due to the reduced acidity of the CV (and other PH1-PH5-containing compartments, like vacuolinos), the acidity of crude homogenates from *ph* mutant petals is also reduced (de Vlaming et al., 1983; Faraco et al., 2017; Verweij et al., 2008). The homogenate pH of blue-violet *RAB5a*^{OE} petals, by contrast, was similar to that of wild-type petals (Figure 3D), suggesting that reduced acidity of the CV is compensated by increased acidity of other compartments, most likely the vacuolinos where PH5 is now upheld.

Epidermal cells of wild-type petals contain numerous vacuolinos, which accumulate preferentially in the conical tip (Faraco et al., 2017), whereas those from *RAB5a*^{OE} petals contain a lower number of vacuolinos that are increased in size, thereby pushing the anthocyanin-containing CV down to leave the conical cell tip essentially colorless (Figures 3E, 3H, and 3I). In transmission electron micrographs (TEMs), we observed intraluminal vesicles (ILVs) in sections of all four enlarged vacuolinos analyzed (Figure 3I) and at a much lower frequency in vacuolinos (2 vacuolinos out of 37, with 1 or 2 ILVs). In addition, the tip of epidermal cells in *RAB5a*^{OE} petals had a rounder shape, associated with increased cell width at 4 μm below the tip, as compared to the more pointed tips of wild-type cells (Figures 3I–3L). In protoplasts from the *RAB5a*^{OE} petal epidermis, transiently expressed-PH5-GFP arrived

Figure 4. A loss-of-function *rab5a* mutation abolished vacuolinos and affects epidermal cell shape

(A) Schematic representation of the *rab5a*^{X2043} allele. Exons are indicated by black rectangles, introns by a thin line, and the inactivating 283 bp *dTPH1* transposon with a red triangle.

(B) Quantitative real-time PCR analysis of the expression of *RAB5a*, *RAB5a1*, and *RAB5a2* in *rab5a*^{X2043} and isogenic WT petals at flower stage 6 (opened flower with closed anthers). Values are shown as mean ± SD (n = 3 biological replicates × 2 technical replicates) and normalized based on the reference gene *PhRAN*. Statistical significance was assessed by Student's t test/Mann-Whitney rank sum test; $^{**}p < 0.01$.

(C) Stage 7 (2 days after flower opening) flowers of *RAB5a*$^{+/+}$ and *rab5a*^{X2043} plants. Scale bars, 1 cm.

(D) Light micrographs and TEM images of petal sections and environmental scanning electron micrographs (ESEMs) of the surface of petals from line R182 (*RAB5a*$^{+/+}$) and R182 individuals homozygous for the *rab5a*^{X2043} mutation. Scale bars for light microscopy are 20 μm, for TEM are 5 μm, and for ESEM are 50 μm. Red asterisks mark the tip of the cells.

(E) Dimensions (height, basal width [n > 100] and apical width [width of 4 μm from the cell tip, n > 80]) of epidermal cells from different lines. Boxplot elements: center line, median; box limits, upper and lower quartiles; whiskers, 1.5× interquartile range; diamonds, outliers. Statistical significance was assessed by Student's t test/Mann-Whitney rank sum test; $^{***}p < 0.001$.

(F) Simplified model of the effect of vacuolinos on dimensions and shape of petal epidermal cells of the same genotypes as above.

(G) Confocal micrographs of *RAB5a*$^{+/+}$ and *rab5a*^{X2043} petal protoplasts transiently expressing PH5-GFP and RFP-SYP122. The number of *RAB5a*$^{+/+}$ epidermal cells imaged at 24 h ($n_{epi\text{-}24h}$) and 48 h ($n_{epi\text{-}48h}$) is 69 and 31, respectively; and the number of mesophyll cells imaged at 24 h ($n_{mes\text{-}24h}$) and 48 h ($n_{mes\text{-}48h}$) is 29 and 24, respectively. For *rab5a*^{X2043} $n_{epi\text{-}24h} = 52$, $n_{mes\text{-}24h} = 21$, $n_{epi\text{-}48h} = 122$, and $n_{mes\text{-}48h} = 35$ cells. The white dotted line indicates the slice chosen for the scans of the intensity of GFP (tonoplast) and RFP (plasma membrane) shown on the right. Bars, 10 μm.

Autofluorescence of anthocyanins is shown in blue, fluorescence of the plasma membrane marker RFP-SYP122 in red, and fluorescence of PH5-GFP in green. 3× Enlargement shows the region marked by the white dashed square at 3-fold larger magnification. Abbreviation: p, puncta. See also Figure S6.

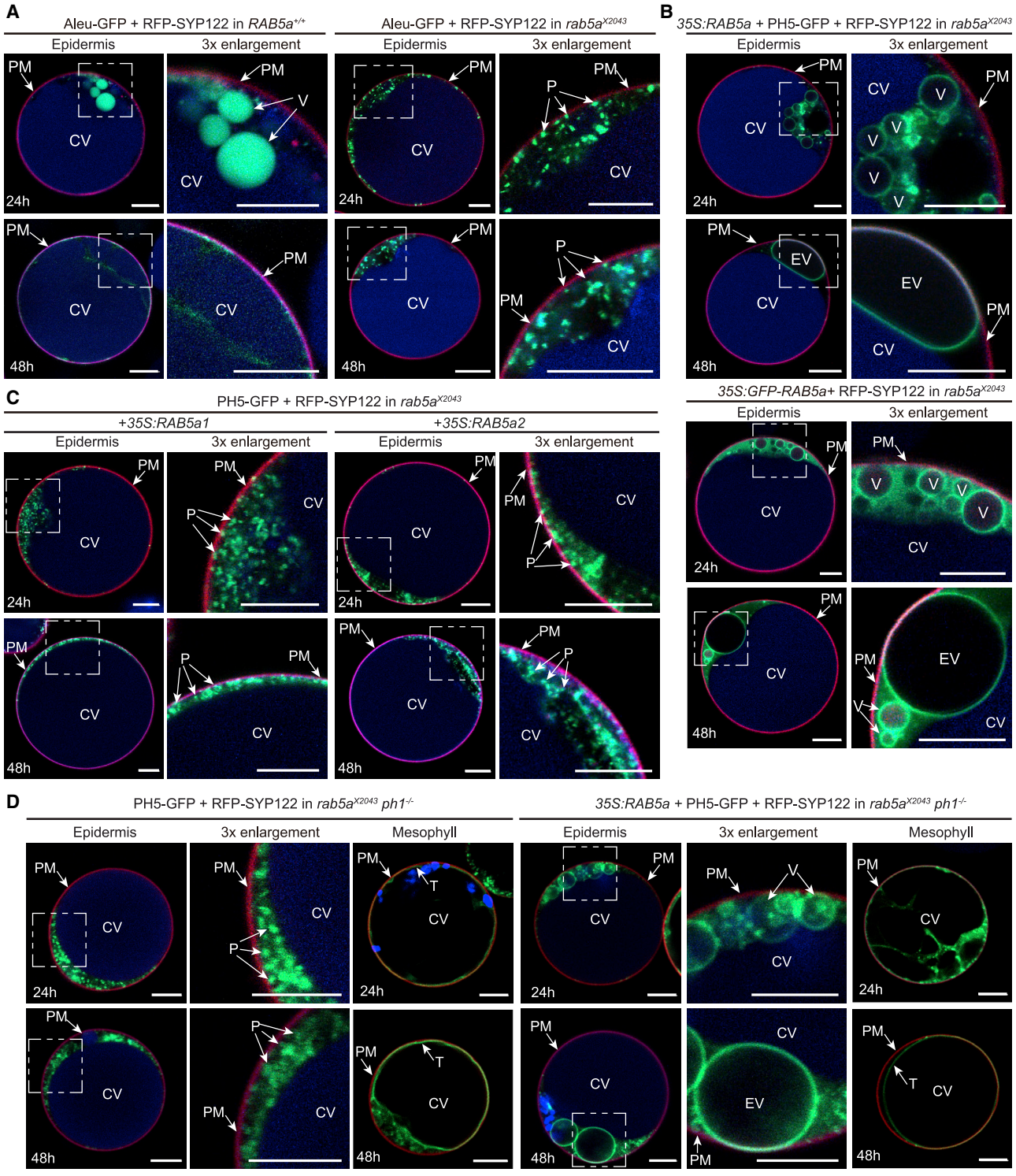

Figure 5. The *rab5a*^{X2043} mutation blocks vacuolino formation and delivery of proteins to the central vacuole in epidermal petal cells

(A) Confocal micrographs of transiently expressed Aleu-GFP in *RAB5a*$^{+/+}$ and *rab5a*^{X2043} petal protoplasts. The number of epidermal *RAB5a*$^{+/+}$ cells imaged after 24h ($n_{epi\text{-}24h}$) and 48h ($n_{epi\text{-}48h}$) is 35 and 28, respectively. For *rab5a*^{X2043}, $n_{epi\text{-}24h}$ = 48, and $n_{epi\text{-}48h}$ = 53 cells.

(B) Transient expression of *35S:RAB5a* or *GFP-RAB5a* in protoplasts from petals of the *rab5a*^{X2043} mutant. For *35S:RAB5a*, $n_{epi\text{-}24h}$ = 72 and $n_{epi\text{-}48h}$ = 51 cells; and for *GFP-RAB5a,* $n_{epi\text{-}24h}$ = 34 and $n_{epi\text{-}48h}$ = 27 cells.

(legend continued on next page)

after 24 h in the (enlarged) vacuolinos, but little or no PH5-GFP arrived at the CV after 48 h (Figure 3F), similar to wild-type cells transiently expressing *35S:RAB5a*. Also in stably transformed plants expressing *35S:GFP-RAB5a*, vacuolinos in most of the petal epidermis were much larger than vacuolinos in control plants expressing *35S:PH5-GFP* (Figures 3G and 3H). The prolonged presence of PH5-GFP (Figure 3F), and endogenous PH1 and PH5, on vacuolinos and the reduced trafficking to the CV will delay the acidification of the CV, explaining the blue-violet petal color when the flower opens, while also enhancing the acidification of vacuolinos, explaining why the overall acidity of *RAB5a*^{OE} petals is not altered.

Effects of the loss of RAB5a function

To further assess the function of RAB5a, we obtained 2 transgenic M1xV30 plants (out of 15 transformants) in which *RAB5a* was about 3-fold downregulated by RNAi (Figures S6D and S6E). In addition, we identified among the progeny of line W138 a mutant allele, *rab5a*^{X2043}, in which a *dTPH1* transposon disrupts the coding sequence 252 bp downstream of the ATG (Figure S6F; Figure 4A) and strongly reduces the amount of *RAB5a* transcripts, without affecting *RAB5a1* and *RAB5a2* mRNA levels (Figure 4B). Petals from *rab5a*^{X2043} homozygotes had a similar color as *RAB5a*$^{+/+}$ siblings in the same background (W138) (Figure 4C), but the epidermal cells lacked vacuolinos. Furthermore, the height and width of the cells, measured at the base of the cell and 4 μm below the tip, were reduced (Figures 4D–4G). Downregulation of *RAB5a* by RNAi also reduced the height of epidermal cells but had, in contrast to *rab5a*^{X2043}, little or no effect on the width at the cell base and significantly increased the width at 4 μm below the tip (Figures 3I–3L). The latter might be an effect from the reduced cell height because the width at 4 μm below the tip now measures the width of "main body" of the cell rather than the tip. The different effect of *rab5a*^{X2043} and *RAB5a*^{RNAi} on (apical) cell width might stem from the somewhat different shape of the epidermal cells in the W138 (*rab5a*^{X2043}) and M1xV30 (*RAB5a*^{RNAi}) genetic background (compare the scanning electron micrographs [SEMs] in Figures 3I and 4D) and/or the strength of the mutation (knockout versus knockdown).

To investigate how *rab5a*^{X2043} affects the sorting of vacuolar proteins, we transiently expressed PH5-GFP or Aleu-GFP in petal protoplasts isolated from *rab5a*^{X2043} homozygotes. In this genetic background (W138), PH5-GFP and Aleu-GFP reached vacuolinos within 24 h after transformation and the CV after 48 h in *RAB5a*$^{+/+}$ petal cells (Figures 4G and 5A), as previously observed for wild-type cells in the M1xV30 genetic background (Faraco et al., 2017). However, in epidermal petal cells of *rab5a*^{X2043} siblings, PH5-GFP and Aleu-GFP labeled 24 h after transformation punctate structures instead of vacuolinos, and only a small fraction reached the CV 48 h after transformation (Figures 4G and 5A). In petal mesophyll cells from *rab5a*^{X2034} mutant and *RAB5a*$^{+/+}$ siblings, PH5-GFP and Aleu-GFP reached the CV directly within 24 h after transformation, as in the M1xV30 wild type (Figures 4G and 5A; Figure S6K). We obtained similar results in the *RAB5a*^{RNAi} knockdown line (Figure S6G) and in lines containing the *rab5a*^{X2043} allele in a distinct genetic background accumulating malvidin anthocyanin (Figures S6H and S6I). Thus, *rab5a*^{X2043} specifically affects the vacuolino pathway in epidermal petal cells and has no effect on the direct pathway to CV that is active in other cells.

When we co-transformed *rab5a*^{X2043} petal protoplasts with *35S:RAB5a* along with *35S:PH5-GFP*, we observed that transient *RAB5a* expression promptly restored the sorting of PH5-GFP to vacuolinos within 24 h after transformation (Figure 5B; Figure S6J). Transient expression of GFP-RAB5a rescued vacuolino formation with similar efficiency (Figure 5B). Some of these rescued cells contained enlarged vacuolinos and showed a delayed delivery of PH5-GFP to the CV, similar to wild-type M1xV30 petal cells expressing *35S:RAB5a* or *35S:GFP-RAB5a* (Figures 3B, 3F, and 3H). The expression of *35S:RAB5a* or *35S:GFP-RAB5a* had no effect on the delivery of PH5-GFP to reach CV in *rab5a*^{X2043} petal mesophyll cells (Figure S6L). Co-transformation of *35S:RAB5a1* or *35S:RAB5a2* did not rescue PH5-GFP trafficking by vacuolinos (Figure 5C), in contrast to *35S:RAB5a* and *35S:GFP-RAB5a*, indicating that RAB5a1 and RAB5a2 are functionally distinct from RAB5a.

Mutation of *PH1* blocks trafficking from vacuolinos to the CV and results in enlarged vacuolinos (Faraco et al., 2017). To better position the function of RAB5a in the vacuolino pathway, we transiently expressed PH5-GFP in petal protoplasts from the *rab5a ph1* double mutant (Figure 5D). In epidermal protoplasts from *rab5a ph1* petals, PH5-GFP remains stuck on puncta, where it is still visible 48 h after transformation (as in *rab5a* cells), instead of labeling vacuolinos and after 48 h the CV (as in wild-type) or enlarged vacuolinos (as in *ph1*). Transient expression of *RAB5a* in *rab5a ph1* petal epidermis protoplasts restored the presence of vacuolinos (rescue of the *rab5a* defect) but did not rescue the defect in trafficking to the CV caused by *ph1* (Figure 5D). This finding indicates that *RAB5a* acts upstream of *PH1* in the vacuolino pathway.

To characterize the PH5-GFP-positive puncta in RAB5a-deficient epidermal petal cells and thereby gain insight into the origin of vacuolinos, we co-transformed *RAB5a*^{RNAi} petal protoplasts with constructs expressing PH5-GFP and RFP- or CHERRY-tagged markers for different cell compartments (Figure 6;

(C) Transient expression of *35S:RAB5a1* or *35S:RAB5a2* in *rab5a*^{X2043} petal protoplasts. For *35S:RAB5a1*, $n_{epi\text{-}24h}$ = 48 and $n_{epi\text{-}48h}$ = 33 cells. For *35S:RAB5a2*, $n_{epi\text{-}24h}$ = 45 and $n_{epi\text{-}48h}$ = 68 cells.

(D) Confocal images of *rab5a*^{X2043} *ph1*$^{-/-}$ protoplast in which PH5-GFP labels puncta-like structures, whereas *rab5a*^{X2043} *ph1*$^{-/-}$ protoplasts expressing *35S:RAB5a* recruit PH5-GFP to enlarged vacuolinos. The number of *rab5a*^{X2043} *ph1*$^{-/-}$ epidermal cells imaged at 24 h ($n_{epi\text{-}24h}$) and 48 h ($n_{epi\text{-}48h}$) is 46 and 65; and the number of mesophyll cells imaged at 24 h ($n_{mes\text{-}24h}$) and 48 h ($n_{mes\text{-}48h}$) is 9 and 7 respectively. For *rab5a*^{X2043} *ph1*$^{-/-}$ cells expressing*35S:RAB5a*, $n_{epi\text{-}24h}$ = 21, $n_{mes\text{-}24h}$ = 6 cells, $n_{epi\text{-}48h}$ = 37, and $n_{mes\text{-}48h}$ = 4 cells).

In all the panels, autofluorescence of anthocyanins in the CV of epidermal cells and chloroplasts in mesophyll cells is shown in blue; fluorescence of RFP-SYP122 in red; and fluorescence of Aleu-GFP, PH5-GFP, and GFP-RAB5a in green. 3× Enlargement shows the region marked by the white dashed square at a 3-fold larger magnification. Bars, 10 μm. See also Figure S6.

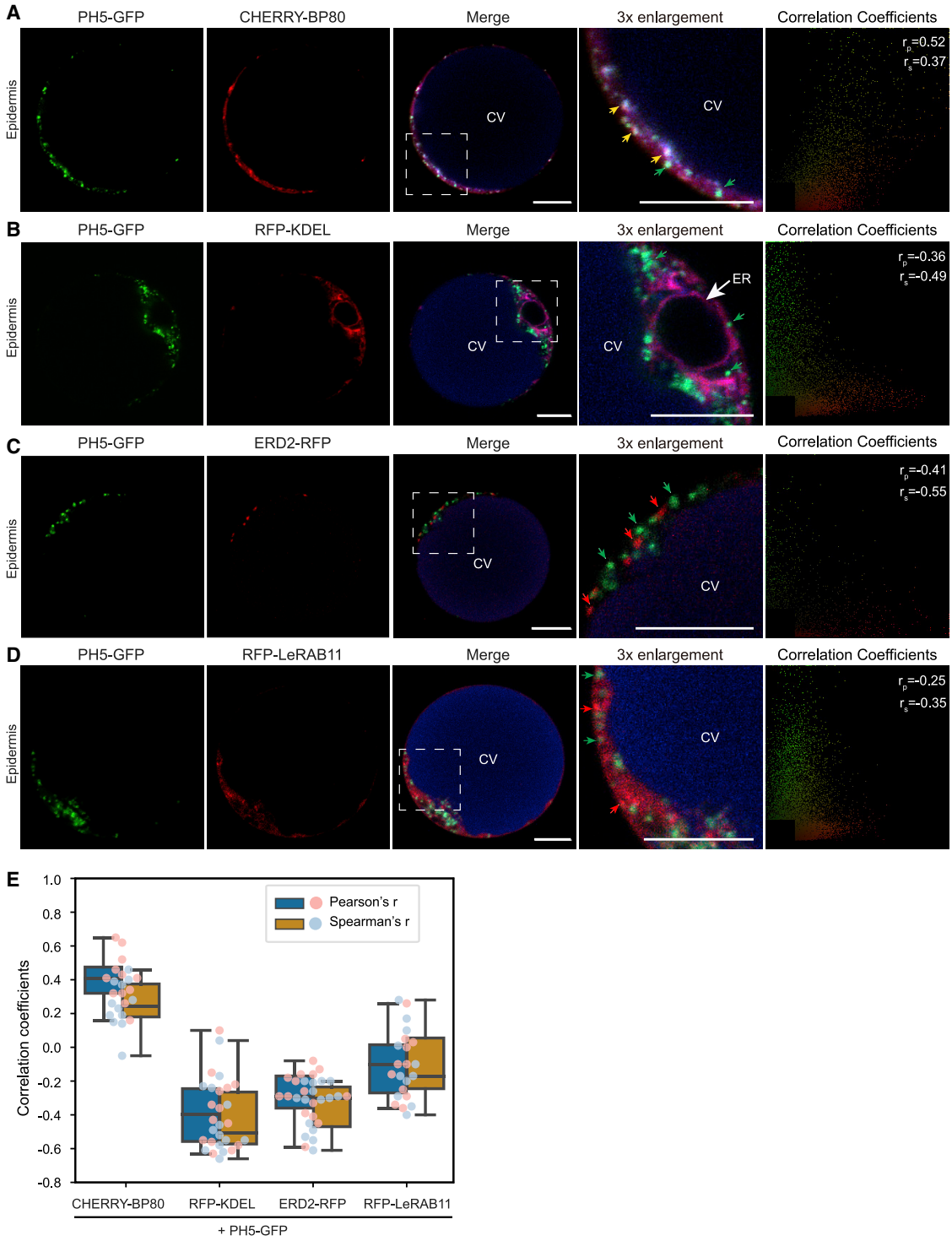

Figure 6. PH5-GFP-positive puncta accumulating in *RAB5a*^{RNAi} petal epidermis are a sub-population of PVCs

(A–D) Confocal pictures of protoplasts derived from the *RAB5a* knockdown mutant (*RAB5a*^{RNAi}) transiently expressing PH5-GFP together with PVC/MVB marker CHERRY-BP80 (A). Confocal pictures of protoplasts derived from the *RAB5a* knockdown mutant transiently expressing PH5-GFP together with RFP-KDEL, a marker for the ER (B); ERD2-RFP, a marker for *cis*-Golgi membranes (C); and RFP-LeRAB11, a marker for the TGN/EE membranes (D). The scatterplots on the right show a correlation of localization patterns, which are expressed as r_p and r_s correlation coefficients. Autofluorescence of anthocyanins is shown in blue, fluorescence of RFP in red, and fluorescence of GFP in green. Size bars, 10 μm in all panels; 3× enlargement shows the region marked by the white dashed

(legend continued on next page)

Figures S7A–S7D). In these experiments, PH5-GFP labeled puncta in epidermal petal cells, as in *rab5a* protoplasts expressing PH5-GFP alone, indicating that none of the FP-tagged marker proteins altered PH5-GFP localization (Figure 6). We observed no co-localization of PH5-GFP with RFP-KDEL, ERD2-RFP, or RFP-LeRAB11 in either epidermal or mesophyll cells of *RAB5a*^{RNAi} petals (Figures 6B–6E; Figures S7B–S7D). However, we did observe (partial) co-localization of PH5-GFP with CHERRY-BP80 (PVCs/MVBs marker) in a sub-population of puncta (Figures 6A and 6E). Together, these results indicate that PVCs/MVBs constitute a heterogeneous population of compartments, at least in the petal epidermis of petunia, and that the PH5-GFP-positive puncta in epidermal cells of *rab5a*^{X2043} (or *RAB5a*^{RNAi}) petals represent a subset of PVCs/MVBs (Figure 4G).

In leaf cells, PVCs are MVBs that become enlarged PVCs (ePVCs) by homotypic fusions after treatment with the phosphoinositide 3-kinase (PI3K) inhibitor wortmannin (Tse et al., 2004; Wang et al., 2009; Zheng et al., 2014). To study if and how wortmannin affects the vacuolino pathway, we transiently expressed CHERRY-BP80 and GFP-RAB5a or PH5-GFP in petal protoplasts and exposed cells 24 h after transformation for 30 min to 16.5 μM wortmannin. In mesophyll cells from wild-type (M1xV30) petals, CHERRY-BP80 and GFP-RAB5a localized again to overlapping populations of puncta, which develop after wortmannin treatment into larger ePVC-like compartments that contain both CHERRY-BP80 and GFP-RAB5a, most likely through homotypic fusion (Figure S7E). We observed similar ePVC-like structures in the wortmannin-treated epidermal cells but also in untreated epidermal cells (possibly induced by GFP-RAB5a), which made it difficult to assess the effect, if any, of wortmannin (Figure S7E). To circumvent this problem, we examined mutant petals. In *ph4* petal protoplasts, GFP-RAB5a and CHERRY-BP80 label small puncta that convert upon wortmannin treatment into larger ePVC-like structures in both mesophyll and epidermal cells (Figures 7A and S7F). In *rab5a*^{X2043} epidermal cells, PH5-GFP and CHERRY-BP80 accumulated again in partially overlapping sets of puncta, which upon wortmannin treatment formed larger ePVC-like structures containing both CHERRY-BP80 and PH5-GFP (Figure 7B), supporting the idea that these puncta resemble PVC-like compartments.

DISCUSSION

Previous findings indicated that the MBWW transcription factor complex PH4-AN1-AN11-PH3 activates a tissue-specific trafficking pathway to the CV by vacuolinos (Faraco et al., 2017). Here, we further characterized this pathway and identified the first MBWW target gene, namely, *RAB5a*, that is involved in the formation of vacuolinos. RAB5a represents an ancient previously unrecognized clade of "canonical" RAB5s that diverged from the well-studied RHA1/ARA7 homologs by changes in its transcriptional regulation, intracellular localization, and biological function, providing a rare example in support of the hypothesis that the diversification and the increased complexity of membrane trafficking during evolution was facilitated by duplication and neo-functionalization of genes encoding key factors like RAB GTPases and SNAREs (Dacks and Field, 2007; Dacks et al., 2008; Sanderfoot, 2007; Schlacht et al., 2014).

Our findings suggest a model (Figure 7C) in which vacuolinos originate from the RAB5a-mediated fusion of a sub-population of PVCs to form larger structures, which also receive (FM4-64 positive) membrane material from the plasma membrane by distinct RAB5a-negative endosomes. In epidermal protoplasts from wild-type petals, we could indeed observe fusion events among PH5-GFP-labeled vacuolinos (Video S1). As RAB5a is necessary to send proteins to vacuolinos but not sufficient to rescue *ph4* (not shown), we infer that other MBWW-regulated factors are involved, of which some act before RAB5a in the vacuolino pathway, at or close to the point where it diverges from the ubiquitous direct pathway(s) to the CV. Thus, in *an1*, *ph3*, and *ph4* mutants, the vacuolino pathway is blocked at an early point from which proteins can be redirected into the direct pathway to the CV, whereas in *rab5a* mutants, proteins are upheld at a later step in the vacuolino pathway, after a "point of no return" (in small PVC-like compartments) from where they cannot be redirected anymore.

The vacuolino pathway displays striking differences and similarities with trafficking pathways to (incipient) vacuoles in leaf, root, and/or suspension cells (Cui et al., 2020; Figure 7C). The most distinguishing feature is that the formation of vacuolinos and subsequent vacuolino-to-CV transport require MBWW-target genes like *RAB5a* and *PH1* that are inactive in leaves and roots (and petal mesophyll) or even missing in *Arabidopsis*. Yet, there are also striking similarities at the microscopic level. In root cortex cells, vacuoles form *de novo* from multivesicular PVCs that fuse into small vacuoles (~1 μm) that grow by additional fusions into a large CV (Cui et al., 2019). The vacuolino pathway also generates *de novo* new secondary vacuoles, but this happens in a late stage of petal development, long after these cells form the large CV. Whether or not these vacuolino precursors are multivesicular is currently unknown. Vacuolinos do contain ILVs at low numbers and at much higher numbers in enlarged vacuolinos in *RAB5a*^{OE} cells. It is, however, unclear whether these ILVs originate from MVB precursors or the internalization of vesicles from the vacuolino membrane, by microautophagy, as part of a degradation process (Yang et al., 2020), or both.

The rapid enlargement of the RAB5-positive compartments after wortmannin treatment indicates that PI3K negatively regulates their homotypic fusion, as it does for PVCs/MVBs in root and leaf cells (Cui et al., 2019; Tse et al., 2004; Wang et al., 2009; Zheng et al., 2014). Expression of the constitutively active (GTP-fixed) ARA7^{Q69L} in leaf and suspension cells also triggered the formation of ePVCs/MVBs (Jia et al., 2013; Kotzer et al., 2004). This (superficially) resembles events along the vacuolino pathway on two points. The first point is the formation of

square at a 3-fold larger magnification. Yellow arrowheads indicate co-localization; red and green arrowheads indicate the absence of co-localization. Abbreviation: ER, endoplasmic reticulum.

(E) Quantification of r_p and r_s colocalization coefficients between PH5-GFP and different organelle markers (n = 11 to 15 cells). See also Figure S7.

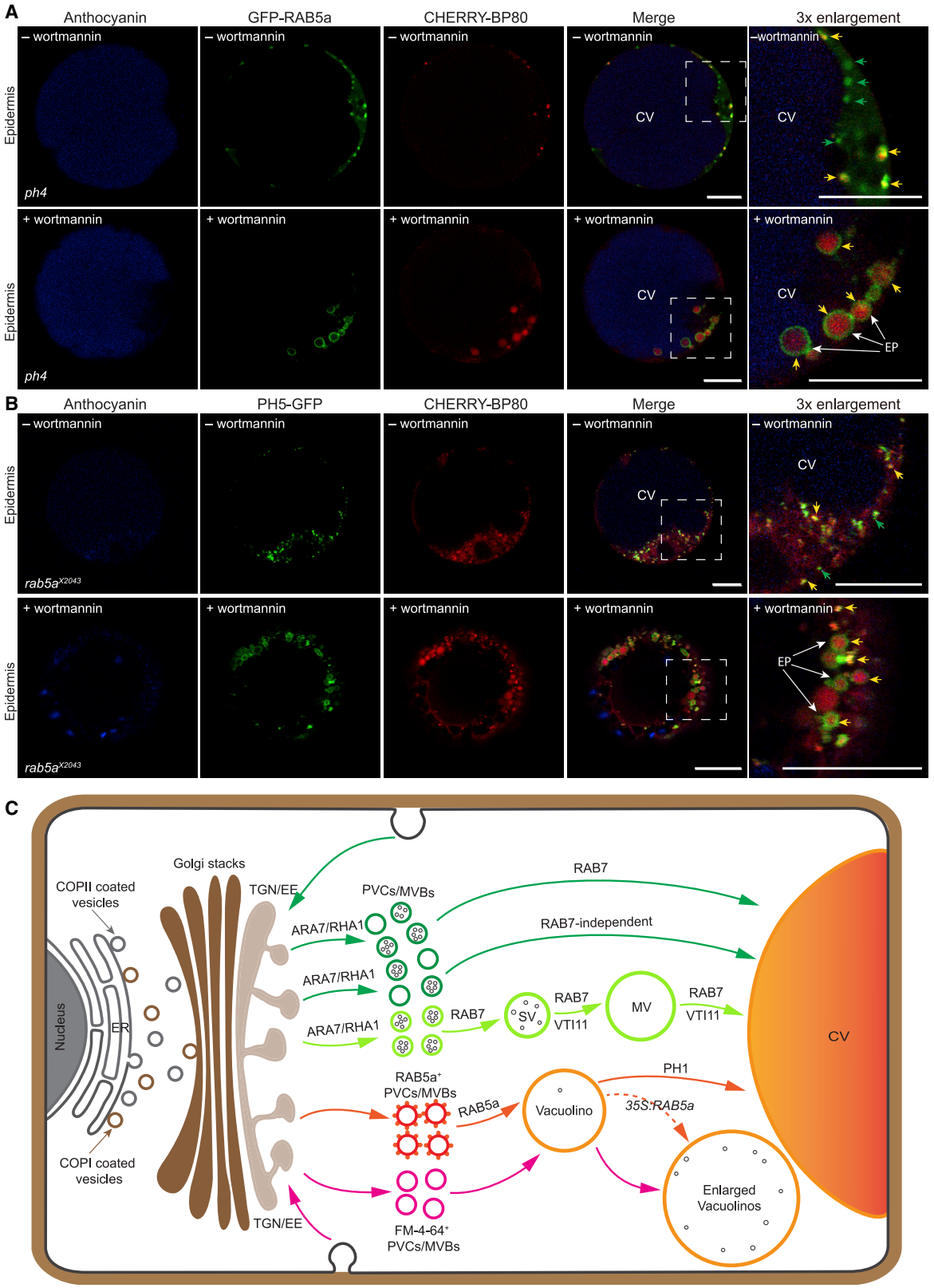

(legend on next page)

vacuolinos through fusions of the small punctate precursors, except that this process is mediated by (native) RAB5a, which is lacking in *Arabidopsis*. The second point is the formation of enlarged vacuolinos and in cells expressing RAB5a or RAB5a2 from the *35S* promoter, which is correlated with and possibly a consequence of the reduced (or delayed) trafficking from vacuolinos to the CV. However, as the last process requires the P_{3B}-ATPase PH1, which is lacking in *Arabidopsis*, the similarities at a microscopic level are likely to rest on (partially) different molecular mechanisms.

The formation of enlarged vacuolinos by *RAB5a*^{OE} shows that a cell may generate multiple vacuoles with distinct function, content, and/or size solely by regulating the temporal expression of RAB5s without a need for specific sorting domains that send proteins to one vacuole or the other. Epidermal petal cells in young petunia flower buds already contain a CV, which during further development to stage 5 (maximum size bud), accumulates, amongst others, anthocyanins. Expression of *MBWW* genes and their targets, such as *RAB5a*, sets in later when anthocyanin synthesis is ceasing, because of which the newly formed vacuolinos are largely devoid of anthocyanins and other compounds and proteins that are synthesized only in earlier stages. Upon prolonged *35S*-driven *RAB5a* expression, the vacuolinos become enlarged, in some cells to a similar or larger size than the CV, becoming essentially an additional anthocyanin-less (central) vacuole that co-exists with the older anthocyanin-containing CV.

Although vacuolinos are an attractive model with which to study membrane trafficking by genetic approaches, their biological function remains to be solved. Vacuolinos may affect optical features of the colored petal cells, which are important for the attraction of pollinators, by excluding the anthocyanin-containing CV from the conical tip and by altering cell dimensions. In *Arabidopsis* petals, the orientation of cortical microtubules is important to give epidermal cells the correct domed shape (Ren et al., 2017), and the formation of vacuolinos might add to shaping epidermal cells, possibly by providing mechanical force. However, vacuolinos may also exist in other cell types, suggesting additional functions, as *RAB5a* is also expressed in the vasculature of petunia leaves and in *Citrus* fruits. In the latter, AN1 drives expression of *PH1* and *PH5* to hyperacidify the CV of juice cells (Strazzer et al., 2019), as well as a *RAB5* gene (Cs1g14330/orange1.1g029103m) (Huang et al., 2016) that is homologous to petunia *RAB5a* (Figure 1E). Whether or not vacuolinos may serve as a sorting station, to prevent selected proteins from reaching the CV, is currently under investigation. Our findings reported here and elsewhere (Faraco et al., 2017) suggest that further analysis of flower color mutants and additional AN1-PH3-PH4 regulated genes is likely to uncover additional factors and mechanisms involved in membrane trafficking that could not be predicted by other approaches.

STAR★METHODS

Detailed methods are provided in the online version of this paper and include the following:

- KEY RESOURCES TABLE
- RESOURCE AVAILABILITY
  - Lead contact
  - Materials availability
  - Data and code availability
- EXPERIMENTAL MODEL AND SUBJECT DETAILS
- METHOD DETAILS
  - Plant material
  - RNA extraction and quantitative real-time PCR
  - Genes and constructs
  - Phylogenetic analysis and sequence alignment
  - Protoplast transformation and confocal microscopy
  - FM4-64 imaging
  - Wortmannin treatment
  - Yeast two hybrid and bimolecular fluorescence complementation (BiFC) assay
  - Light microscopy and transmission electron microscopy of petal sections
  - Environmental scanning electron microscopy
  - GUS Staining
  - Western blotting
- QUANTIFICATION AND STATISTICAL ANALYSIS

SUPPLEMENTAL INFORMATION

Supplemental information can be found online at https://doi.org/10.1016/j.celrep.2021.109749.

ACKNOWLEDGMENTS

Authors are in debt with the staff of the LCAM (Van Leeuwenhoek Centre for Advanced Microscopy) of the University of Amsterdam for their assistance with technical issues during the microscopic observation. We want to thank Jihed Chouaref for help with the preparation of figures. We are grateful to

Figure 7. Wortmannin treatment induces the formation of enlarged PVCs

(A) Confocal images of protoplasts derived from *ph4* mutant petals co-expressing GFP-RAB5a and CHERRY-BP80, treated with 16.5 μM wortmannin.

(B) Confocal images of protoplasts isolated from a *rab5a*^{X2043} petal co-expressed with PH5-GFP and CHERRY-BP80, which was treated with 16.5 μM wortmannin.

(A and B) Autofluorescence of anthocyanins is shown in blue, fluorescence of RFP-SYP122 in red, and fluorescence of PH5-GFP as well as GFP-RAB5a in green. Size bars, 10 μm in all panels. 3× Enlargement shows the region marked by the white dashed square at a 3-fold larger magnification. Yellow arrowheads indicate co-localization, and green arrowheads indicate the absence of co-localization.

(C) Schematic representation of the RAB5a-mediated pathway for vacuolino formation. Dark-green arrows denote two "direct" canonical protein sorting pathways to CV observed in a variety of cells (Cui et al., 2020; Ebine et al., 2014). A very similar direct pathway operates in petal mesophyll cells and petal epidermis cells from mutants with a defective MBWW complex. Light-green arrows denote a pathway involved in vacuolar biogenesis in developing root cells (Cui et al., 2019). Orange arrows denote the vacuolino pathway in which *RAB5a* promotes fusions among PVCs and pre-vacuolinos prior to the PH1-dependent trafficking from vacuolinos to the CV. Overexpression of *RAB5a* from the *35S* promoter induces the formation of enlarged vacuolinos by promoting fusions among PVCs and vacuolinos and inhibiting further trafficking to the CV, as indicated by the dashed arrow. The possible route for endocytosis of FM4-64 in petal epidermal cells generated from *GFP-RAB5a*^{OE} plant or WT petunia is indicated by magenta arrows. Intraluminal vesicles (ILVs) are depicted as small black circles. Abbreviations: EP, enlarged PVCs; SV, small vacuole; MV, medium vacuole. See also Figure S7 and Video S1.

Pieter Hoogeveen and Bets Verbree for the care of the Amsterdam Petunia Collection.

This publication is part of the project PH2: a kinase controlling vacuolar acidification in plant cells (with project number ALWOP.222 of the research programme Earth and Life Sciences open program) which is (partly) financed by the Dutch Research Council (NWO), and was in addition supported by a CNRS ATIP-AVENIR grant to M.V. and fellowships to S.L. (China Scholarship Council and EMBO short-term fellowship 7867), Y.L. (China Scholarship Council), and E.M.-C. (European Fellowship programme Erasmus+).

AUTHOR CONTRIBUTIONS

S.L. performed most of the experimental work. P.S., M.B., Y.L., C.S., E.M.-C., and B.L. helped in some experiments. L.R. and M.C. performed the light microscopy, TEM, and ESEM analysis. M.V. isolated the transposon insertion mutant *rab5a*^{X2043}, and F.M.Q. and R.K. conceived this project. S.L., F.M.Q., and R.K. wrote the paper.

DECLARATION OF INTERESTS

Authors declare to have no competing financial interests.

Received: January 12, 2021
Revised: June 11, 2021
Accepted: September 2, 2021
Published: September 28, 2021

REFERENCES

Barr, F., and Lambright, D.G. (2010). Rab GEFs and GAPs. Curr. Opin. Cell Biol. *22*, 461–470.

Bottanelli, F., Gershlick, D.C., and Denecke, J. (2012). Evidence for sequential action of Rab5 and Rab7 GTPases in prevacuolar organelle partitioning. Traffic *13*, 338–354.

Carney, D.S., Davies, B.A., and Horazdovsky, B.F. (2006). Vps9 domain-containing proteins: activators of Rab5 GTPases from yeast to neurons. Trends Cell Biol. *16*, 27–35.

Cui, Y., Cao, W., He, Y., Zhao, Q., Wakazaki, M., Zhuang, X., Gao, J., Zeng, Y., Gao, C., Ding, Y., et al. (2019). A whole-cell electron tomography model of vacuole biogenesis in Arabidopsis root cells. Nat. Plants *5*, 95–105.

Cui, Y., Zhao, Q., Hu, S., and Jiang, L. (2020). Vacuole biogenesis in plants: how many vacuoles, how many models? Trends Plant Sci. *25*, 538–548.

Dacks, J.B., and Field, M.C. (2007). Evolution of the eukaryotic membrane-trafficking system: origin, tempo and mode. J. Cell Sci. *120*, 2977–2985.

Dacks, J.B., Poon, P.P., and Field, M.C. (2008). Phylogeny of endocytic components yields insight into the process of nonendosymbiotic organelle evolution. Proc. Natl. Acad. Sci. USA *105*, 588–593.

De Benedictis, M., Bleve, G., Faraco, M., Stigliano, E., Grieco, F., Piro, G., Dalessandro, G., and Di Sansebastiano, G.P. (2013). AtSYP51/52 functions diverge in the post-Golgi traffic and differently affect vacuolar sorting. Mol. Plant *6*, 916–930.

de Vetten, N., Quattrocchio, F., Mol, J., and Koes, R. (1997). The *an11* locus controlling flower pigmentation in petunia encodes a novel WD-repeat protein conserved in yeast, plants, and animals. Genes Dev. *11*, 1422–1434.

de Vlaming, P., Schram, A.W., and Wiering, H. (1983). Genes affecting flower colour and pH of flower limb homogenates in *Petunia hybrida*. Theor. Appl. Genet. *66*, 271–278.

Dereeper, A., Guignon, V., Blanc, G., Audic, S., Buffet, S., Chevenet, F., Dufayard, J.-F., Guindon, S., Lefort, V., Lescot, M., et al. (2008). Phylogeny.fr: robust phylogenetic analysis for the non-specialist. Nucleic Acids Res. *36*, W465–W469.

Di Sansebastiano, G.P., Paris, N., Marc-Martin, S., and Neuhaus, J.M. (2001). Regeneration of a lytic central vacuole and of neutral peripheral vacuoles can be visualized by green fluorescent proteins targeted to either type of vacuoles. Plant Physiol. *126*, 78–86.

Ebine, K., Fujimoto, M., Okatani, Y., Nishiyama, T., Goh, T., Ito, E., Dainobu, T., Nishitani, A., Uemura, T., Sato, M.H., et al. (2011). A membrane trafficking pathway regulated by the plant-specific RAB GTPase ARA6. Nat. Cell Biol. *13*, 853–859.

Ebine, K., Inoue, T., Ito, J., Ito, E., Uemura, T., Goh, T., Abe, H., Sato, K., Nakano, A., and Ueda, T. (2014). Plant vacuolar trafficking occurs through distinctly regulated pathways. Curr. Biol. *24*, 1375–1382.

Epimashko, S., Meckel, T., Fischer-Schliebs, E., Lüttge, U., and Thiel, G. (2004). Two functionally different vacuoles for static and dynamic purposes in one plant mesophyll leaf cell. Plant J. *37*, 294–300.

Faraco, M., Di Sansebastiano, G.P., Spelt, K., Koes, R.E., and Quattrocchio, F.M. (2011). One protoplast is not the other!. Plant Physiol. *156*, 474–478.

Faraco, M., Spelt, C., Bliek, M., Verweij, W., Hoshino, A., Espen, L., Prinsi, B., Jaarsma, R., Tarhan, E., de Boer, A.H., et al. (2014). Hyperacidification of vacuoles by the combined action of two different P-ATPases in the tonoplast determines flower color. Cell Rep. *6*, 32–43.

Faraco, M., Li, Y., Li, S., Spelt, C., Di Sansebastiano, G.P., Reale, L., Ferranti, F., Verweij, W., Koes, R., and Quattrocchio, F.M. (2017). A tonoplast P_{3B}-ATPase mediates fusion of two types of vacuoles in petal cells. Cell Rep. *19*, 2413–2422.

Fleurat-Lessard, P., Frangne, N., Maeshima, M., Ratajczak, R., Bonnemain, J.L., and Martinoia, E. (1997). Increased expression of vacuolar aquaporin and H^+-ATPase related to motor cell function in *Mimosa pudica* L. Plant Physiol. *114*, 827–834.

Fluckiger, R., De Caroli, M., Piro, G., Dalessandro, G., Neuhaus, J.M., and Di Sansebastiano, G.P. (2003). Vacuolar system distribution in *Arabidopsis* tissues, visualized using GFP fusion proteins. J. Exp. Bot. *54*, 1577–1584.

French, A.P., Mills, S., Swarup, R., Bennett, M.J., and Pridmore, T.P. (2008). Colocalization of fluorescent markers in confocal microscope images of plant cells. Nat. Protoc. *3*, 619–628.

Frigerio, L., Hinz, G., and Robinson, D.G. (2008). Multiple vacuoles in plant cells: rule or exception? Traffic *9*, 1564–1570.

Fukuda, M., Wen, L., Satoh-Cruz, M., Kawagoe, Y., Nagamura, Y., Okita, T.W., Washida, H., Sugino, A., Ishino, S., Ishino, Y., et al. (2013). A guanine nucleotide exchange factor for Rab5 proteins is essential for intracellular transport of the proglutelin from the Golgi apparatus to the protein storage vacuole in rice endosperm. Plant Physiol. *162*, 663–674.

Goh, T., Uchida, W., Arakawa, S., Ito, E., Dainobu, T., Ebine, K., Takeuchi, M., Sato, K., Ueda, T., and Nakano, A. (2007). VPS9a, the common activator for two distinct types of Rab5 GTPases, is essential for the development of *Arabidopsis thaliana*. Plant Cell *19*, 3504–3515.

Grant, S.G., Jessee, J., Bloom, F.R., and Hanahan, D. (1990). Differential plasmid rescue from transgenic mouse DNAs into Escherichia coli methylation-restriction mutants. Proc. Natl. Acad. Sci. USA *87*, 4645–4649.

Herman, E.K., Ali, M., Field, M.C., and Dacks, J.B. (2018). Regulation of early endosomes across eukaryotes: Evolution and functional homology of Vps9 proteins. Traffic *19*, 546–563.

Holland, P.W., Marlétaz, F., Maeso, I., Dunwell, T.L., and Paps, J. (2017). New genes from old: asymmetric divergence of gene duplicates and the evolution of development. Philos. Trans. R. Soc. Lond. B Biol. Sci. *372*, 20150480.

Holsters, M., de Waele, D., Depicker, A., Messens, E., van Montagu, M., and Schell, J. (1978). Transfection and transformation of Agrobacterium tumefaciens. Mol. Gen. Genet. *163*, 181–187.

Huang, D., Zhao, Y., Cao, M., Qiao, L., and Zheng, Z.-L. (2016). Integrated systems biology analysis of transcriptomes reveals candidate genes for acidity control in developing fruits of sweet orange (*Citrus sinensis* L. Osbeck). Front. Plant Sci. *7*, 486.

James, P., Halladay, J., and Craig, E.A. (1996). Genomic libraries and a host strain designed for highly efficient two-hybrid selection in yeast. Genetics *144*, 1425–1436.

Jia, T., Gao, C., Cui, Y., Wang, J., Ding, Y., Cai, Y., Ueda, T., Nakano, A., and Jiang, L. (2013). ARA7(Q69L) expression in transgenic Arabidopsis cells induces the formation of enlarged multivesicular bodies. J. Exp. Bot. *64*, 2817–2829.

Kotzer, A.M., Brandizzi, F., Neumann, U., Paris, N., Moore, I., and Hawes, C. (2004). AtRabF2b (Ara7) acts on the vacuolar trafficking pathway in tobacco leaf epidermal cells. J. Cell Sci. *117*, 6377–6389.

Landt, O., Grunert, H.-P., and Hahn, U. (1990). A general method for rapid site-directed mutagenesis using the polymerase chain reaction. Gene *96*, 125–128.

Langemeyer, L., Perz, A., Kümmel, D., and Ungermann, C. (2018). A guanine nucleotide exchange factor (GEF) limits Rab GTPase-driven membrane fusion. J. Biol. Chem. *293*, 731–739.

Larkin, M.A., Blackshields, G., Brown, N.P., Chenna, R., McGettigan, P.A., McWilliam, H., Valentin, F., Wallace, I.M., Wilm, A., and Lopez, R. (2007). Clustal W and Clustal X version 2.0. Bioinformatics *23*, 2947–2948.

Lee, G.-J., Sohn, E.J., Lee, M.H., and Hwang, I. (2004). The *Arabidopsis* rab5 homologs rha1 and ara7 localize to the prevacuolar compartment. Plant Cell Physiol. *45*, 1211–1220.

Letunic, I., Khedkar, S., and Bork, P. (2021). SMART: recent updates, new developments and status in 2020. Nucleic Acids Res. *49*, D458–D460.

Müller, M.P., and Goody, R.S. (2018). Molecular control of Rab activity by GEFs, GAPs and GDI. Small GTPases *9*, 5–21.

Nicholas, K.B. (1997). GeneDoc: analysis and visualization of genetic variation. Embnet News *4*, 14.

Nielsen, M.E., and Thordal-Christensen, H. (2018). Loss of VPS9b enhances *vps9a-2* phenotypes. Plant Signal. Behav. *13*, e1445950.

Nielsen, M.E., Jürgens, G., and Thordal-Christensen, H. (2017). VPS9a activates the Rab5 GTPase ARA7 to confer distinct pre-and postinvasive plant innate immunity. Plant Cell *29*, 1927–1937.

Otegui, M.S., Noh, Y.S., Martínez, D.E., Vila Petroff, M.G., Staehelin, L.A., Amasino, R.M., and Guiamet, J.J. (2005). Senescence-associated vacuoles with intense proteolytic activity develop in leaves of Arabidopsis and soybean. Plant J. *41*, 831–844.

Paris, N., Stanley, C.M., Jones, R.L., and Rogers, J.C. (1996). Plant cells contain two functionally distinct vacuolar compartments. Cell *85*, 563–572.

Quattrocchio, F., Wing, J., van der Woude, K., Souer, E., de Vetten, N., Mol, J., and Koes, R. (1999). Molecular analysis of the *anthocyanin2* gene of *petunia* and its role in the evolution of flower color. Plant Cell *11*, 1433–1444.

Quattrocchio, F., Verweij, W., Kroon, A., Spelt, C., Mol, J., and Koes, R. (2006). PH4 of Petunia is an R2R3 MYB protein that activates vacuolar acidification through interactions with basic-helix-loop-helix transcription factors of the anthocyanin pathway. Plant Cell *18*, 1274–1291.

Quattrocchio, F.M., Spelt, C., and Koes, R. (2013). Transgenes and protein localization: myths and legends. Trends Plant Sci. *18*, 473–476.

Rehman, R.U., Stigliano, E., Lycett, G.W., Sticher, L., Sbano, F., Faraco, M., Dalessandro, G., and Di Sansebastiano, G.P. (2008). Tomato Rab11a characterization evidenced a difference between SYP121-dependent and SYP122-dependent exocytosis. Plant Cell Physiol. *49*, 751–766.

Ren, H., Dang, X., Cai, X., Yu, P., Li, Y., Zhang, S., Liu, M., Chen, B., and Lin, D. (2017). Spatio-temporal orientation of microtubules controls conical cell shape in *Arabidopsis thaliana* petals. PLoS Genet. *13*, e1006851.

Rutherford, S., and Moore, I. (2002). The *Arabidopsis* Rab GTPase family: another enigma variation. Curr. Opin. Plant Biol. *5*, 518–528.

Sanderfoot, A. (2007). Increases in the number of SNARE genes parallels the rise of multicellularity among the green plants. Plant Physiol. *144*, 6–17.

Schlacht, A., Herman, E.K., Klute, M.J., Field, M.C., and Dacks, J.B. (2014). Missing pieces of an ancient puzzle: evolution of the eukaryotic membrane-trafficking system. Cold Spring Harb. Perspect. Biol. *6*, a016048.

Silva-Alvim, F.A.L., An, J., Alvim, J.C., Foresti, O., Grippa, A., Pelgrom, A., Adams, T.L., Hawes, C., and Denecke, J. (2018). Predominant Golgi residency of the plant K/HDEL receptor is essential for its function in mediating ER retention. Plant Cell *30*, 2174–2196.

Sohn, E.J., Kim, E.S., Zhao, M., Kim, S.J., Kim, H., Kim, Y.W., Lee, Y.J., Hillmer, S., Sohn, U., Jiang, L., and Hwang, I. (2003). Rha1, an Arabidopsis Rab5 homolog, plays a critical role in the vacuolar trafficking of soluble cargo proteins. Plant Cell *15*, 1057–1070.

Spelt, C., Quattrocchio, F., Mol, J.N., and Koes, R. (2000). *anthocyanin1* of petunia encodes a basic helix-loop-helix protein that directly activates transcription of structural anthocyanin genes. Plant Cell *12*, 1619–1632.

Stabentheiner, E., Zankel, A., and Pölt, P. (2010). Environmental scanning electron microscopy (ESEM)—a versatile tool in studying plants. Protoplasma *246*, 89–99.

Strazzer, P., Spelt, C.E., Li, S., Bliek, M., Federici, C.T., Roose, M.L., Koes, R., and Quattrocchio, F.M. (2019). Hyperacidification of *Citrus* fruits by a vacuolar proton-pumping P-ATPase complex. Nat. Commun. *10*, 744.

Sunada, M., Goh, T., Ueda, T., and Nakano, A. (2016). Functional analyses of the plant-specific C-terminal region of VPS9a: the activating factor for RAB5 in Arabidopsis thaliana. J. Plant Res. *129*, 93–102.

Tse, Y.C., Mo, B., Hillmer, S., Zhao, M., Lo, S.W., Robinson, D.G., and Jiang, L. (2004). Identification of multivesicular bodies as prevacuolar compartments in *Nicotiana tabacum* BY-2 cells. Plant Cell *16*, 672–693.

Ueda, T., Yamaguchi, M., Uchimiya, H., and Nakano, A. (2001). Ara6, a plant-unique novel type Rab GTPase, functions in the endocytic pathway of *Arabidopsis thaliana*. EMBO J. *20*, 4730–4741.

Ueda, T., Uemura, T., Sato, M.H., and Nakano, A. (2004). Functional differentiation of endosomes in Arabidopsis cells. Plant J. *40*, 783–789.

Uemura, T., and Ueda, T. (2014). Plant vacuolar trafficking driven by RAB and SNARE proteins. Curr. Opin. Plant Biol. *22*, 116–121.

Vernoud, V., Horton, A.C., Yang, Z., and Nielsen, E. (2003). Analysis of the small GTPase gene superfamily of Arabidopsis. Plant Physiol. *131*, 1191–1208.

Verweij, W., Spelt, C., Di Sansebastiano, G.P., Vermeer, J., Reale, L., Ferranti, F., Koes, R., and Quattrocchio, F. (2008). An H^+ P-ATPase on the tonoplast determines vacuolar pH and flower colour. Nat. Cell Biol. *10*, 1456–1462.

Verweij, W., Spelt, C.E., Bliek, M., de Vries, M., Wit, N., Faraco, M., Koes, R., and Quattrocchio, F.M. (2016). Functionally similar WRKY proteins regulate vacuolar acidification in Petunia and hair development in Arabidopsis. Plant Cell *28*, 786–803.

Wandinger-Ness, A., and Zerial, M. (2014). Rab proteins and the compartmentalization of the endosomal system. Cold Spring Harb. Perspect. Biol. *6*, a022616.

Wang, J., Cai, Y., Miao, Y., Lam, S.K., and Jiang, L. (2009). Wortmannin induces homotypic fusion of plant prevacuolar compartments. J. Exp. Bot. *60*, 3075–3083.

Yang, X., Zhang, W., Wen, X., Bulinski, P.J., Chomchai, D.A., Arines, F.M., Liu, Y.-Y., Sprenger, S., Teis, D., Klionsky, D.J., and Li, M. (2020). TORC1 regulates vacuole membrane composition through ubiquitin- and ESCRT-dependent microautophagy. J. Cell Biol. *219*, e201902127.

Zheng, J., Han, S.W., Rodriguez-Welsh, M.F., and Rojas-Pierce, M. (2014). Homotypic vacuole fusion requires VTI11 and is regulated by phosphoinositides. Mol. Plant *7*, 1026–1040.

STAR★METHODS

KEY RESOURCES TABLE

REAGENT or RESOURCE	SOURCE	IDENTIFIER
Antibodies		
GFP (FL): sc-8334	Santa Cruz Biotechnology	Lot # C2614; RRID:AB_641123
Anti-Rabbit IgG (H+L), HRP Conjugate	Promega	Cat # W4011; RRID:AB_430833
Bacterial and virus strains		
Agrobacterium tumefaciens	Holsters et al., 1978	N/A
E. coli DH10B	Grant et al., 1990	N/A
Critical commercial assays		
iTaq Universal SYBR® Green Supermix	BIO-RAD	Cat # 172-5121
Phusion High-Fidelity DNA Polymerase	Thermo Fisher SCIENTIFIC	Cat # F-530XL
Invitrogen M-MLV Reverse Transcriptase	Thermo Fisher SCIENTIFIC	Cat # 28025013
Gateway BP Clonase Enzyme Mix	Thermo Fisher SCIENTIFIC	Cat # 11789013
Gateway LR Clonase II Enzyme mix	Thermo Fisher SCIENTIFIC	Cat # 11791100
ECL Prime Western Blotting System	GE Healthcare Life Science	Cat # GERPN2232
SynaptoRed C2	Sigma-Aldrich	Cat # S6689
Cellulase onozuka R-10	Duchefa Biochemie	Lot # 016309.01
Macerozyme	Duchefa Biochemie	Lot # 015810.01
Gamborg's B-5 basal salt	SIGMA	Lot # SLCB4231
Wortmannin	LC Laboratories®	Cat # W-2990
Deposited data		
RNaseq data	This study	Genbank: Bioproject PRJNA753066
RAB5a mRNA	This study	Genbank: MH986793
RAB5a1 mRNA	This study	Genbank: MH986794
RAB5a2 mRNA	This study	Genbank: MH986795
PhARA6 mRNA	This study	Genbank: MK896357
PhVPS9 mRNA	This study	Genbank: MK896358
Experimental models: Organisms/strains		
P. hybrida W138	Spelt et al., 2000	N/A
P. hybrida R182 (*rab5a*^{X2042})	This study	N/A
P. hybrida W225 (*an1*^{W225})	Spelt et al., 2000	N/A
P. hybrida R162 *(ph4)*	Quattrocchio et al., 2006	N/A
P. hybrida R167 *(ph3)*	Verweij et al., 2016	N/A
P. hybrida V23 (ph1)	Faraco et al., 2014	N/A
P. hybrida M1xV30	Amsterdam Petunia collection	N/A
35S:RAB5a in *P. hybrida* M1xV30	This study	N/A
35S:GFP-RAB5a in *P. hybrida* M1xV30	This study	N/A
35S: RAB5a^{RNAi} in *P. hybrida* M1xV30	This study	N/A
35S: PH5-GFP in *P. hybrida* M1xV30	This study	N/A
proRAB5a:GFP-GUS in *P. hybrida* M1xV30	This study	N/A
Saccharomyces cerevisiae PJ69	James et al., 1996	N/A
Oligonucleotides		
Please see Table S2 N/A		
Software and algorithms		
MUSCLE	Dereeper et al., 2008	http://www.atgc-montpellier.fr/phyml/
PHYML	Dereeper et al., 2008	http://www.atgc-montpellier.fr/phyml/

(*Continued on next page*)

Continued

REAGENT or RESOURCE	SOURCE	IDENTIFIER
ClustalX 2.1	Larkin et al., 2007	http://www.clustal.org/clustal2/
GeneDoc 2.7	Nicholas, 1997	N/A
SigmaPlot 12.0	Systat Software Inc.	https://systatsoftware.com/
Adobe Illustrator CS6	Adobe Inc.	https://www.adobe.com/
Python3	N/A	https://www.python.org/
QuantStudio Design Analysis Software v1.5.1	Thermo Fisher SCIENTIFIC	https://www.thermofisher.com/us/en/home.html
Seaborn 0.11.1	N/A	https://seaborn.pydata.org/
CellSens image analysis software	OLYMPUS	https://www.olympus-lifescience.com/
ZEN 2.1 (blue edition)	ZEISS	https://www.zeiss.com/corporate/int/home.html
ImageJ	N/A	https://imagej.nih.gov/ij/download.html
PSC plug-in for ImageJ	French et al., 2008	http://www.nottingham.ac.uk/research/groups/cvl/software/

RESOURCE AVAILABILITY

Lead contact

Requests for further information and/or resources should be directed to and will be fulfilled by the lead contact, Ronald Koes (ronald.koes@uva.nl).

Materials availability

All materials generated in this study are available from the lead contact.

Data and code availability

Sequence data generated in this study were deposited in the National Center for Biotechnology Information (NCBI) under Bioproject Genbank: PRJNA753066 (RNaseq data) and accession numbers Genbank: MH986793 (*RAB5a* mRNA), Genbank: MH986794 (*RAB5a1* mRNA), Genbank: MH986795 (*RAB5a2* mRNA), Genbank: MK896357 (*PhARA6* mRNA), and Genbank: MK896358 (*PhVPS9* mRNA).

This paper does not report original code

Any additional information required to reanalyze the data reported in this work paper is available from the Lead Contact upon request.

EXPERIMENTAL MODEL AND SUBJECT DETAILS

The wild-type *P. hybrida* accessions used for plant and protoplast transformation were the F1 hybrid M1xV30 or a homozygous $AN1^{+}$ revertant of the inbred line *P. hybrida* W138 that was maintained in line R175. The transposon insertion mutant $rab5a^{X2042}$ was isolated and maintained in the $AN1^{+}$ revertant W138 background. For the expression analyses in Figure 1 we used the inbred *P. hybrida* lines R175 (wt), R162 (*ph4*), and R167 (*ph3*), which were all in an $AN1^{+}$ revertant W138 genetic background (Quattrocchio et al., 2006; Verweij et al., 2016) and line W225 (*an1*) containing a stable recessive *an1* allele derived from $an1^{W138}$.

All Petunia plants used in this work were grown in a greenhouse under normal conditions (19°C /30°C min/max, with cycles of 16/8 hours light/dark in summer, and with cycles of additional illumination of 15/9 hours light/dark in winter).

METHOD DETAILS

Plant material

Petunia line R182 ($rab5a^{X2043}$) is a transposon insertion mutant for *RAB5a* in the W138 line. The (transformable) F1 hybrid M1xV30 (wild-type) was used to generate stable transformants. V23 ($ph1^{v23}$) is a petunia line harboring a stable *ph1* allele disrupted by a 7-bp transposon footprint in the coding sequence. The *rab5a*/*ph1* double mutant was isolated by PCR screening of the F2 progeny from the cross R182 ($rab5a^{X2043}$) X V23 ($ph1^{v23}$). A $rab5a^{X2043}$ mutant in a malvidin background was isolated from the F2 of the cross of R182 ($rab5a^{X2043}$) with the wild-type line V30. Transgenic plants expressing *35S:RAB5a*, *35S:GFP-RAB5a*, *35S:PH5-*

GFP and plants expressing *proRAB5a:GFP-GUS* were obtained by *Agrobacterium tumefaciens*-mediated leaf disc transformation of the F1 hybrid M1xV30 (wild-type). *RAB5a*^{RNAi} knock down lines were generated by RNA interference in the F1 hybrid M1xV30 (wild-type).

RNA extraction and quantitative real-time PCR

Total RNA was isolated from petunia tissues using the TRIzol reagent (Thermo Fisher Scientific). Quantitative real-time PCR was performed with an iTaq Universal SYBR Green kit (Bio-Rad) using primers listed in Table S1 and an Applied Biosystems QuantStudio 3 Real-Time PCR System and QuantStudio Design Analysis Software.

Genes and constructs

RAB5a coding sequence (CDS) was amplified from M1xV30 (wild-type) petal *cDNAs* with primer 7253 and 7254 containing *att*B1 and *att*B2 sites using Phusion® High-Fidelity DNA Polymerase; Purified *RAB5a* CDS was subsequently cloned into Gateway® pDONR221 donor vector as an entry clone by Gateway® BP recombination reaction (Invitrogen Clonase Gateway BP Clonase II Enzyme Mix); Finally Gateway® LR recombination reaction (Invitrogen Clonase Gateway LR Clonase II Enzyme Mix) were performed with *RAB5a* CDS entry clone and multiple destination vectors (Table S2) to make functional plasmids for several purpose. By using the same procedures, CDS of *RAB5a1* (primer 7602 + 7603), *RAB5a2* (primer 7607 + 7608), *PhARA6* (primer 7577 + 7578) and *PhVPS9a* (primer 7508 + 7509) were amplified and subsequently subcloned into multiple destination vectors (Table S2). Promoter sequence of *RAB5a* (primer 7513+7514) obtained from wild-type petal *gDNA* with Phusion® High-Fidelity DNA Polymerase, cloned into Gateway® pDONR221 donor vector, and recombined with destination vector pKGWFS7 to drive the expression of *GFP* and *GUS*. Constitutively active (GTP-bound) and constitutive negative (GDP-bound) mutants of *RAB5s* were generated by PCR based site-directed mutagenesis (Landt et al., 1990). The GDP-bound mutant of *RAB5a* termed *RAB5a*^{T24N} for example was generated as follows: forward primer (7253), containing an *att*B1 site, and a reverse primer (7656) containing the desired mutation (mutating amino acid T (Threonine) to N (Asparagine)) were used in a first round of PCR with Phusion® High-Fidelity DNA Polymerase. The resulting PCR product was used as forward primer together with reverse primer (7254), containing an *att*B2 site, in a second PCR reaction. Products of this second PCR reaction were cloned into the Gateway® pDONR207 donor, sequenced and subsequently transferred by Gateway recombination into multiple types of destination vectors for functional constructs (Table S2). For *RAB5a* RNA interference (RNAi), a target sequence containing partial the last exon and 3′utr were amplified with primers (7854+7855), which were cloned into Gateway® pDONR221 donor vector and pK7GWIWG2 (I) binary silencing vector.PH5-GFP was identified as marker for vacuolinos membrane and tonoplast of CV (Faraco et al., 2017); RFP-SYP122 has been described as plasma membrane (PM) marker, detailed description of how these plasmids were made published before (Faraco et al., 2017). Aleu-GFP (Aleu = the first 431 bases of the CDS of the barley aleurain cDNA) was previously used as marker for the lumen of central vacuole (Di Sansebastiano et al., 2001) and vacuolino (Faraco et al., 2017). ERD2-RFP were constructed by amplifying (primers 7474 + 7475) the CDS of *ERD2* cDNA of *A. thaliana* and subcloning it into the Gateway destination vector pK7RWG2,0 by BP and LR reactions. RFP-KDEL (Faraco et al., 2017), RFP-LeRAB11 (Rehman et al., 2008) and CHERRY:BP80 (BP80 = the transmembrane domain/cytoplasmic tail sequence of the BP80 cDNA) (De Benedictis et al., 2013; Tse et al., 2004) were described in previous works. All the primers used in this study are reported in Table S1. Vectors applied in this study are presented in Table S2.

Phylogenetic analysis and sequence alignment

Amino acid sequences of RAB5 homologs from different plant species were selected from the Petunia Genome SGN dedicated database (https://solgenomics.net/), Phytozome databases (https://phytozome-next.jgi.doe.gov/), PLAZA (https://bioinformatics.psb.ugent.be/plaza/), and Ensembl (http://www.ensembl.org//useast.ensembl.org/?redirectsrc=//www.ensembl.org%2F). Multiple sequences alignments were conducted by MUSCLE. The phylogenetic tree was produced by maximum-likelihood using the online tool PhyML 3.0 (http://www.atgc-montpellier.fr/phyml/). G-blocks were applied to curate the alignment and 300 bootstrap replicates were used to assess the branch support (Dereeper et al., 2008). Amino acid sequence alignment was performed by ClustalX version 2.1, and further edited by program GeneDoc version 2.7.

Protoplast transformation and confocal microscopy

Protoplast isolation and transformation was done as described previously with minor modifications (Faraco et al., 2011). Petal limbs from three stage-7 flowers (2 days after bud opening) were sterilized for 30 s in 0.5% hypochlorite in a rooting pot (190ml, 66x68mm, Greiner), rinsed three times in sterile water, transferred to a Petri dish (94x16 mm, with vents, Greiner Bio-One B.V.) containing 2 mL filter-sterilized TEX buffer (3.1g/L Gamborg's B-5 basal salt mixture, 1.28mM MES, 6.8mM $CaCl_2$*$2H_2O$, 1.32mM NH_4NO_3, and 0.4M sucrose, pH 5.7, sterilize with 0.45 μm sterile syringe filter) containing 0.2% (w/v) macrozyme R-10, and 0.4% (w/v) cellulase onozuka R-10, gently sliced petals using a sterile scalpel. After addition of another 8 mL digestion solution (0.2% (w/v) macrozyme R-10, and 0.4% (w/v) cellulase R-10 in TEX buffer) the sliced petals were incubated overnight at room temperature in the dark. The next morning protoplasts were released by gently lifting the digested petal pieces up and down with a forceps and passed through a 100 μm nylon mesh to remove undigested tissue and other debris. After addition of 15 mL freshy prepared TEX buffer, the protoplast suspension is transferred to a 50mL centrifuge tube and spun for 10 min at 100 g in a swing out rotor with deceleration set at zero. Using a long Pasteur pipette (230 mm) connected to an electronic pipette controller by a pipette tip(1mL), a piece of rubber tube and a serological pipette(25mL), the pelleted debris and as much of the buffer was removed from under the layer of floating live protoplasts. The pro-

toplasts were washed once by adding 25 mL fresh TEX buffer, centrifugation for 10 minutes at 100 g (deceleration set at zero) and removal of the TEX buffer from under the floating protoplasts. After resuspension in 25 mL fresh TEX buffer, protoplasts were then kept on ice for 30 minutes and centrifuged again for 10 min at 100 g. After removal of the TEX buffer and resuspension in 3-5 mL (depending on the amount of protoplast) of MMM solution (0.5M Mannitol, 15mM $MgCl_2$, and 0.1% MES) protoplasts are ready for transformation.

For one transformation, 20 μg plasmid DNA, 300 μL protoplast suspension and 300 μl PEG solution (0.4M Mannitol, 0.1M $Ca(NO_3)_2$, adjusted to pH to 8 before adding 40% PEG4000) were gently mixed in a 12 mL tube for 1 minute. After addition of 2 mL TEX buffer the suspension was gently mixed again and incubated for 1 hour at room temperature. After addition of 5 mL W5 buffer (154 mM NaCl, 125mM $CaCl_2$, 5 mM KCl, 5 mM Glucose, pH 5.7) and gentle mixing, protoplasts are pelleted at 100 g for 10 minutes, and resuspended in 2 mL TEX buffer and incubated for 20-48 hr before microscopic analysis.

Transfected cells were imaged with a Zeiss LSM510 confocal microscope using a 40x/1.2 water objective at 24 or 48 hours after transformation. For GFP and anthocyanins excitation we used a 488nm laser and detection filters BP505-550 and LP650 respectively. For RFP and CHERRY excitation was at 568nm and detection was achieved with a BP585-615 filter. Protoplasts isolated from petals of a stable *35S:PH5-GFP* transgenic line (*PH5-GFP*^{OE}) were loaded into WillCo-dish® Glass Bottom Dishes (HBST-3522) to make movies of the fusion event between vacuolinos by Andor spinning disk confocal microscopy (Nikon TI microscope body equipped with Andor spinning disk and FRAPPA unit for confocal imaging).

FM4-64 imaging

Protoplasts prepared for staining with FM4-64 (SynaptoRed C2, Sigma-Aldrich®) were isolated from petals of transgenic plants expressing 35S:*GFP-RAB5a*. After addition of FM4-64 to a final concentration of 50 μM FM4-64 protoplasts were kept in the dark and imaged after 10 mins, 1 hour, 5 hours, and 24 hours with a Zeiss LSM510 confocal microscope using a 40x/1.2 water objective.

Wortmannin treatment

Protoplasts were isolated from petals of wild-type (M1xV30), *rab5a*^{X2043}, or *ph4* mutants and transiently transformed with plasmids of interest, respectively. 24 hours after transformation, transformed cells were treated with 16.5 μM (final concentration) wortmannin (LC Laboratories®) for 30 mins in the dark. After the treatment, protoplasts were centrifuged, resuspended and kept in fresh buffer for a variable period before imaging with a Zeiss LSM510 confocal microscope using a 40x/1.2 water objective.

Yeast two hybrid and bimolecular fluorescence complementation (BiFC) assay

Yeast two-hybrid assays were performed as reported before (Quattrocchio et al., 2006). In BiFC assays, plasmids encoding N-terminal fusions of protein of interest to nYFP and cYFP and, to mark the plasma membrane of transformed cells, RFP-SYP122 were transformed into protoplasts isolated from petunia M1xV30 (wild-type) petals. Transfected cells were imaged with a Zeiss LSM510 confocal microscope with a 40x/1.2 water objective at 24 hours after transformation. Over hundred transfected cells expressing RFP-SYP122 were observed for each independent experiment, and around 20 cells were imaged by confocal microscopy.

Light microscopy and transmission electron microscopy of petal sections

Semi-thin sections of petal tissue were prepared and observed as previously described (Faraco et al., 2017). Petal limbs at anthesis (stage 6) were fixated for 24 hours in in75 mM sodium cacodylate buffer (pH 7.2) containing 5% (w/v) glutaraldehyde, washed four times for 15 min each in 75 mM cacodylate buffer (pH 7.2), post-fixed for 90 min in 1% (w/v) OsO_4, dehydrated by passage through a series of stepwise increased ethanol concentrations o, and included in resin (Epon, 2-dodecenylsuccinic anhydride, and methylnadic anhydride mixture). Semi- thin sections (1–2 mm) were cut by ultramicrotome (OmU2, Reichert), stained with toluidine blue, and observed under a light microscope (DMLB, Leica Microsystems).

Transmission electron microscopy of petal cells was performed as previously reported (Verweij et al., 2008). Petal tissue from stage 6 flowers (anthesis) was fixed overnight at room temperature in 75 mM cacodylate buffer, pH 7.2 containing 5% (v/v) glutaraldehyde and post-fixed for 4 hours in 75 mM cacodylate buffer, pH 7.2 containing 1% (w/v) OsO_4 for 4 h. After dehydration in a graded ethanol series and propylene oxide, samples were embedded in Epon resin (2-dodecenylsuccinic anhydride and methylnadicanhydrid mixture; Sigma-Aldrich). A pre-inclusion at room temperature in increasing concentrations of resin dissolved in propylene oxide was followed by the final inclusion in freshly prepared resin followed by the polymerization at 35°C for 12 h, 45°C for 12 h, and at 60°C for 12 h. Ultrathin sections were mounted on uncoated copper grids (200 mesh).

Cell dimension measurements were performed on the semi-thin sections of petal tissue. Height of cell was defined as the distance from the cell tip to the base of the cell. Basal width and apical width of cells were measured at the basal end of the cell and at 4 μm down from the cell tip, respectively. All the measurements have been done with CellSens image analysis software.

Environmental scanning electron microscopy

Petal portions were fixed in 0.075M cacodylate buffer (pH 7.2) containing 3% (w/v) glutaraldehyde. Pre-fixed samples were then washed with 0.075M cacodylate buffer (pH 7.2) three times (7 mins each time), which were post-fixed in 0.075M cacodylate buffer (pH 7.2) containing 1% (w/v) OsO4 for 1 hour. Post-fixed samples were further washed three times (7 mins each time) in 0.075M caco-

dylate buffer (pH 7.2) and observed by ESEM (Environmental scanning electron microscopy) in wet mode (Stabentheiner et al., 2010).

GUS Staining

Flowers and leaves of petunia line transformed with *proRAB5a:GFP-GUS* and untransformed line (M1 × V30) were collected and immediately dipped into cold 90% acetone for 20 mins. After removal of acetone by two washes with staining buffer (100mM sodium phosphate buffer (pH 7.2), 0.1% (w/v) Triton X-100 and 10mM EDTA) tissues were transferred to staining buffer containing 2mM X-Gluc (5-Bromo-4-Chloro-3-Indoyl-Beta-D-Glucuronide). To aid penetration of substrate into the tissue, samples were put under vacuum for three times 20 minutes and further incubated at 37°C for several hours till the blue color developed and then transferred to 70% ethanol for long term storage and imaging.

Western blotting

GFP-tagged proteins prepared for western blotting were isolated from wild-type protoplasts transformed with plasmids for the expression of the different protein fusions. Protoplast isolation and transformation protocols (Faraco et al., 2011), as well as western blotting (Verweij et al., 2008) procedures were previously reported.

QUANTIFICATION AND STATISTICAL ANALYSIS

Statistical analysis was performed using SigmaPlot 12.0. The normal distribution of values for all samples was confirmed by using Shapiro-Wilk normality test. Comparisons between two groups were performed using Student's t test if variance was equal (Levene's mean test) or using Mann-Whitney Rank Sum test if variance was unequal. Quantification of colocalization of FP-tagged proteins was performed with the PSC colocalization plugin (French et al., 2008) of the ImageJ.